CHALMERS
UNIVERSITY OF TECHNOLOGY

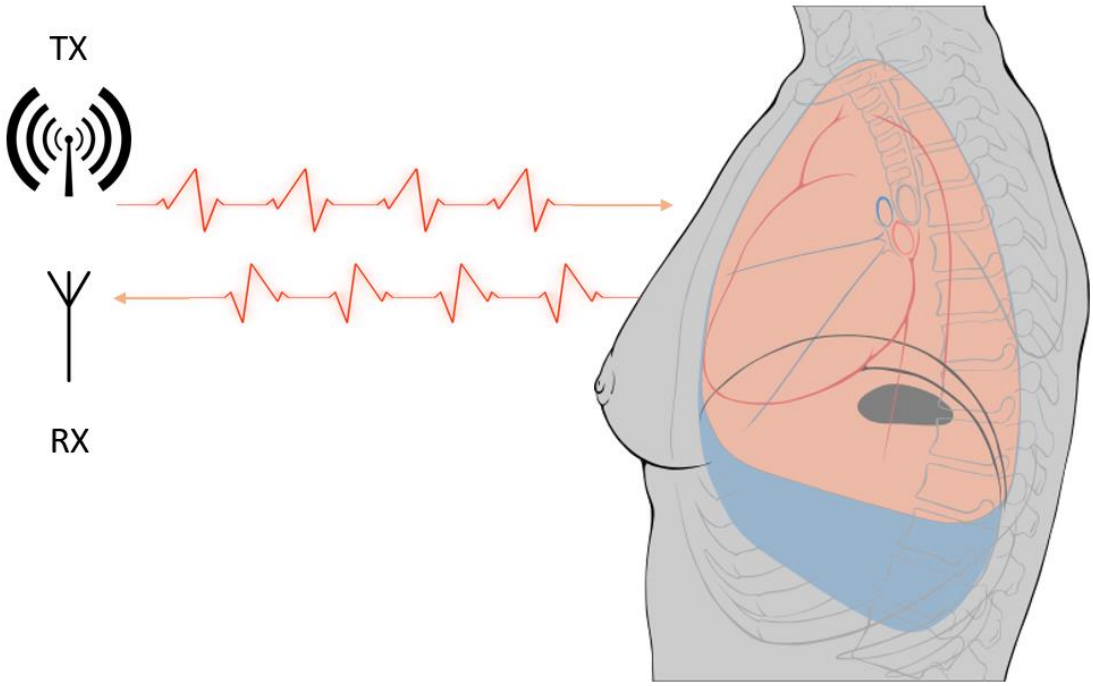

Microwave based Vital Sign Detection and Monitoring

Master's thesis in Biomedical Engineering

JOAKIM ROBAKOWSKI

Department of Electrical Engineering
CHALMERS UNIVERSITY OF TECHNOLOGY
Gothenburg, Sweden 2020

Acknowledgements

First, I want to thank Xuezhi Zeng that has been an amazing supervisor throughout the thesis, and I am grateful for the opportunity of writing my thesis at the department of Electrical Engineering in Chalmers University of Technology. Furthermore, I would like to thank Albert Monteith, Berglind Fridriksdottir and Sigrun Helga Davidsdottir for their support that speeded up the progress of the project.

My main moral support during the studies has been provided by my dearest friends within and outside of the university: Alessandro Cafasso, Ion Olaetxea, Khushwinder Gill, Tom Donder and Saša Stankic. Finally, I want to thank my family for not only supporting me, but also for making this journey possible.

Gothenburg, 2020.
Joakim Robakowski

Abstract

Ultra-Wide Band (UWB) technology has proven to be a reliable option for contact-less detection of the vital signs: breathing rate and heartbeat rate. Both vital signs are considered important in prehospital diagnosis since they can provide critical information needed to make life-saving decisions. Currently, a compact UWB system for medical diagnostics has been developed by a Chalmers team. The aim of the research project is to use this compact system as a mobile equipment in e.g. ambulances, where prehospital diagnosis of medical conditions, such as stroke, can be carried out.

The aim of this project is to investigate if this developed system has the potential to detect the vital signs. In order to detect the movement, a new data recording strategy with a higher speed was proposed and implemented. Simulations were carried out to verify the effectiveness of the signal processing methods as well as determining the essential parameters for measurement settings. Furthermore, measurements were carried out to verify the potential of the measurement system.

Two signal processing methods were used to extract the frequency of the chest displacement. Of the two methods, one turned out to struggle with detection of the heartbeat rate. Tiny chest displacements were not detectable with the settings applied to the receiver. However, the other method could successfully detect breathing rate in 90% of the collected measurements, and in some cases, detect the heartbeat rate repeatedly. The results have shown that the investigated microwave system has the potential to detect the vital signs.

Table of Contents

Abbreviations

ADC	Analog-to-Digital Converter
AWG	Arbitrary Waveform Generator
CW	Continuous Wave
ECG	Electrocardiogram
FPGA	Field-Programmable Gate Array
GUI	Graphical User Interface
LNA	Low Noise Amplifier
PA	Power Amplifier
PLL	Phase Locked Loop
PN	Pseudo-random Noise
PPG	Photopethysmogram
PRBS	Pseudo Random Binary Sequence
RF	Radio Frequency
TOF	Time of Flight
T&H	Track and Hold
UWB	Ultra-Wideband
VAT	Variable Attenuator

1. Introduction

Yearly, almost 800 000 people have a stroke in USA from which 140 000 people die. It creates a substantial economic burden to the society, with an estimated cost of $34 billion each year. Early action is crucial for an effective treatment since every minute counts when stroke happens [1].

Prehospital diagnosis of stroke patients is necessary for early treatment. Microwave based solutions have become strong candidate for prehospital diagnosis applications, and for stroke detection microwaves have proven to be effective. However, there is a lack of commercial solutions for prehospital stroke detection. The reason is that research on biomedical microwave imaging has focused mainly on algorithm development and antenna design, while most of the investigated systems consist of lab instruments. The lab instruments are expensive, inconvenient and impractical. Researchers at Chalmers University of Technology are currently developing a microwave-based diagnostic system. The intention is to use the system for medical diagnosis in ambulances so that the medical personnel can get additional support for triage decision or even initiating some treatment. Besides from stroke diagnosis, the system could be used for detecting different trauma injuries, for instance the chest wall injury [2].

During prehospital diagnosis, the measurement and monitoring of vital sign such as heart rate and breathing rate are also important [3]. They can provide critical information needed to make life-saving decisions.

Nowadays, the most conventional ways to monitor heartbeat rate is either by measuring the electrical activity of the heart, known as electrocardiography (ECG), or by observing the change in blood flow using light, known as photoplethysmography (PPG) [4] [5]. ECG is perhaps the most recognizable method where two or three electrodes are attached to a patient's torso and the measured signal is displayed as a repeating appearance of the QRS-complex.

On the other hand, breathing rate can be measured by using sensors such as optical sensors that detect the variation in humidity between exhaled and inhaled air [6]. But the conventional methods to measure the vital signs have some drawbacks. For instance, the electrodes for ECG that are attached to the patient's skin are not convenient nor adequate for long term monitoring. Additionally, the cabling between the ECG and the electrodes limits the comfort and mobility of the patient [7]. As a consequence of the drawbacks contactless methods have been studied and developed to get around these kinds of limitations, such as camera-based systems for breathing rate or laser-based monitoring systems for heartbeat rate [7] [8].

One of the potential technologies for contactless vital sign monitoring is microwaves. The microwave method is safe, comfortable and easy to use. Its main advantage over laser-based methods is that microwaves can perform monitoring through layers of different materials (tissues, clothes, wall, etc.). Moreover, as the rapid development of microwave integrated circuit technology, the size and cost of microwave electronics have been dramatically reduced, which makes microwave sensors very attractive for long-term health monitoring.

Several studies on using microwaves for vital sign monitoring have been carried out. The systems use either continuous waves (CW) [9] or short microwave pulses [10]. The CW method is based on transmission of a Radio Frequency (RF) single-tone continuous wave signal. The wave is reflected by a target and subsequently acquired by the receiving antenna. The received signal carries information containing physical movements of the measured subject in its phase [9]. Generally, the UWB method

differs in such way that the transmitted signal consists of cyclically transmitted pulse. When the pulses are reflected from the target, the movement of the measured target is determined by the difference in time-of-flight (TOF) of each pulse [10].

In the project, we will investigate a different type of UWB system for vital sign monitoring. This system uses pseudo random binary sequence (PRBS) as the transmitted signal and it was primarily developed for the diagnostics of stroke and trauma by the Chalmers research group.

A fast data recording strategy was proposed and implemented in order to resolve the vital signs. The system transmits a UWB signal towards the subject and from which the signal is reflected. The received signal is then processed in order to extract the desired information, such as the heartbeat rate and breathing rate.

Section 2 of the thesis describes the basic movement properties of a human chest that are caused by breathing and heart beats. It is also described how the path of a reflected signal changes due to chest motion.

In section 3, the hardware of the microwave system is described. The properties of the transmitted signal are described, and the sampling of the received signal is explained.

Section 4 describes the signal processing methods used to detect the vital signs, whereas section 5 describes the performed measurements and presents the results.

Finally, the discussion and conclusion are in section 6 and section 7.

2. Background and Theory

Microwave technology has been explored in different application areas [11]. It has been successfully used to detect the vital sign of a subject, even at a distance of several meters with the body wearing clothes. A typical vital sign detection scenario using microwaves is illustrated in Figure 1. Two antennas (the transmitting and the receiving) are placed at a certain distance to the body under investigation. A microwave signal transmitted to the body will be reflected back and acquired by the receiving antenna. The phase of the body-reflected signal is modulated by the chest wall displacement due to the breathing and heartbeat. Therefore, by extracting the phase variation of the reflected signal, the breathing rate and heartbeat rate can be estimated.

2.1. Chest displacement

Heart beats and breathing contribute to the movement of the chest. The vital signs are distinguishable thanks to the difference in their characteristics. A simple mathematical model of the combined vital signs (vs) was developed to easily obtain and understand the frequency spectrum of the detected vital signs [10]:

$$vs(t) = m_b\, sin(2\pi f_{br} t) + m_h\, sin(2\pi f_{hbr} t) \quad (1)$$

Where the variables mean:

$$\begin{aligned} m_b &= Amplitude\ of\ respiratory\ displacement \\ m_h &= Amplitude\ of\ heartbeat\ displacement \\ f_{br} &= Breathing\ rate \\ f_{hbr} &= Heartbeat\ rate \end{aligned}$$

An estimation of frequency intervals for both f_{br} and f_{hbr} has been made considering scenarios of normal persons [12]:

$$\begin{aligned} f_{br}&: 0.1\ to\ 0.7\ Hz\ (6\ to\ 42\ breaths/min) \\ f_{hbr}&: 0.9\ to\ 3\ Hz\ (54\ to\ 180\ beats/min) \end{aligned}$$

Moreover, the amplitudes of the two vital signs differs significantly where m_b is an arbitrary value in the millimeter range whereas m_h is an amplitude on the order of 0.01mm [13].

2.2. Phase-shifted signal due to chest motion

In microwave-based vital sign detection methods, transmitted signal is directed towards the patient [10] [13]. Figure 1 illustrates how the transmitted signal propagates from one antenna (TX) towards the patient, reflects off the chest of the patient and propagates back and is captured by the receiving antenna (RX).

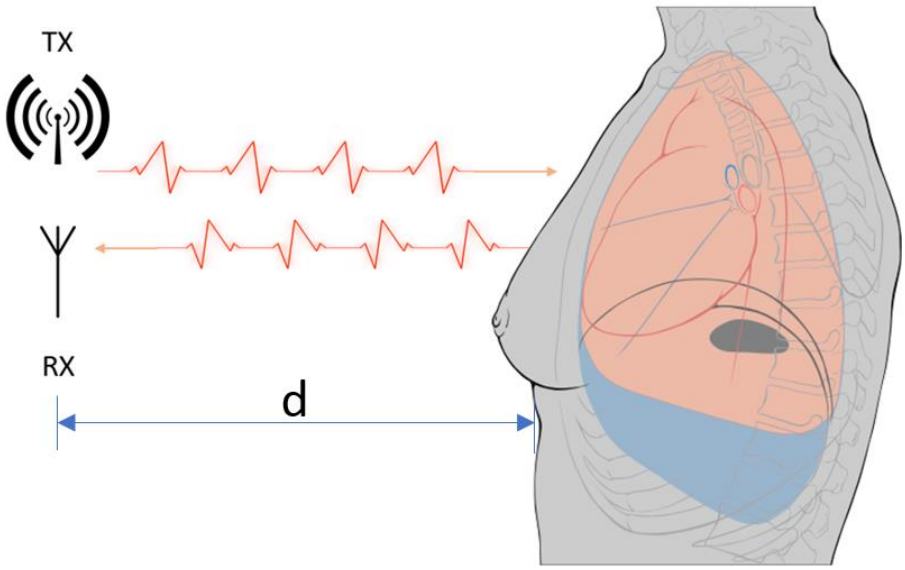

Figure 1. Illustration shows a transmitter antenna (TX) and receiver antenna (RX) to the left, and a human body, also referred to as "subject" in the thesis, to the right. "d" is the distance between the antennas and the subject.

The distance, *d*, between the system and the subject varies continuously due to chest motion, in this case caused by the vital signs. If the distance to the subject is static, which means that the chest is not moving, signals that are transmitted towards the chest will have the same time of flight (TOF). The TOF will change if *d* changes. The change of distance, Δd, can be determined from the following equation:

$$t(i) = time\ instance\ at\ which\ the\ vital\ sign\ amplitude\ was\ measured$$

$$\Delta d(t(i)) = vs(t(i)) - vs(t(i-1)) \quad (2)$$

where $vs(t(i))$ is the chest-displacement caused by the vital signs at the time instance t(i). Assuming that the transmitted signal propagates with the speed of light, *c*, $\tau_d(t(i))$ describes the difference of time that it took for the latest signal to propagate towards the chest and back:

$$\tau_{\mathrm{d}}(t(i)) = 2 \cdot \frac{\Delta d(t(i))}{c} \quad (3)$$

3. Measurement system

The measurement system shown in Figure 2 is designed for medical imaging, specifically a microwave tomography system. The system transmits UWB signals as PN-sequence in the frequency range of 500 MHz – 3 GHz. The bandwidth has been chosen considering several practical issues and using a trade-off between spatial resolution and penetration depth of human tissue. Human tissue is highly lossy and the loss increases with high frequency. However, high frequency gives better image resolution [2].

The transmitter and receiver are hardware synchronized, where both subsystems are indirectly controlled by the same reference clock, f_b, of the PN-sequence generator. Figure 2 shows that the receiver's ADC and T/H are controlled by a frequency f_f, which is synthesized from f_b in the clock generation system. This is described in section 3.1.4 [14]. Considering that the subsystems are synchronous, and that the PN-sequence is repeatedly transmitted, an equivalent time-sampling method has been employed to obtain a suitable effective sampling rate. This sampling method reconstructs one signal from samples taken on consecutive cycles of the measured signal. Each sample is sequentially delayed from the previous sample, meaning that the receivers true sampling rate is slightly lower than the repetition rate of the transmitted signal [2]. The receiver's FPGA collects several reconstructed signals into a data set that is finally transmitted to a PC for processing in order to extract the frequencies of the vital signs.

3.1. Hardware components

The system is mostly the same as used in [14], however without the switching matrix that is mentioned in the paper, as shown in Figure 2.

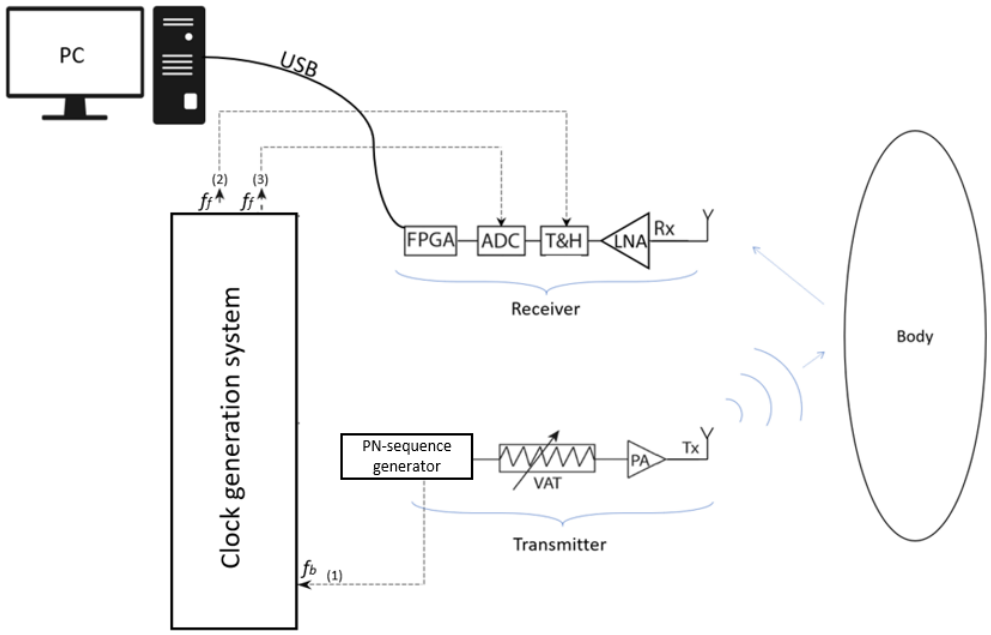

Figure 2. Block diagram of the measurement system hardware. Dashed arrow lines going to the clock generation system represent the reference clock of the clock generation system f_b, (1), and the dashed arrows going out of the clock generation system represent the sampling clocks f_f, (2) and (3). The Field Programmable Gate Array (FPGA) is the data acquisition device that is controlled by the PC and transfers data to the PC for latter signal processing.

Table 1 shows a specific list of components used in the system presented in Figure 2. The list includes the: PN-sequence generator, variable attenuator (VAT), power amplifier (PA), low noise amplifier (LNA), track and hold (T/H), analog-to-digital converted (ADC), a Field-Programmable Gate Array (FPGA) and antennas. The clock-generation system consists of a phase locked loop (PLL) and a clock distributor, described more in [14].

Table 1. Components/equipment of which the system consists of. [14] [15]

Components/Instruments	BW, GHz	Gain or sampling rate
VAT (8495B)	DC-18	0 - (-70) dB
PA (ZHL-42W)	0.01 - 4.2	30 dB
LNA (HMC639ST89E)	0.2 - 4.0	13 dB
T&H (HMC760LC4B)	DC - 5	4 Gsa/s (Max)
ADC (ADS41B29)	DC - 0.6	250 Msa/s (Max)
PLL (ADF4351)	0.035 - 4.4	
Clock distributor (AD9508)	DC - 1.65	
Antennas (non-commercial)	1.5 - 2	
FPGA (ML605)		
PN-sequence generator (ASNTPRBS20)		

3.1.1. Antennas

The non-commercial antennas used in this project were designed to be used in microwave hyperthermia, where the system is designed for a broad frequency range [16]. Bandwidth of the antennas range from approximately 1.5GHz - 2 GHz where the antennas radiate the best at ~1.8GHz [17]. These antennas were used because of two reasons. The first reason is the good directivity of the antennas, meaning that most of the signal power is transmitted in one direction. Secondly, the antennas are small and their surface is flat making it simple to ensure good contact with the body.

Ideally, the bandwidth of the antennas covers the frequency band of the generated signal. If it is not the case, the power of the transmitted signal might be strongly attenuated. As a consequence of that, the signal-to-noise ratio (SNR) will become worse. The properties of the generated signals are described in section 3.2. There it is evident that the antennas bandwidth does not cover the complete frequency band of the PN-sequence. However, the bandwidth of the antennas is not a key issue in microwave-based vital sign detection as the SNR can be improved by amplifying the generated signal before the transmitting antenna.

3.1.2. Transmitter

The PN-sequence generator produces the desired signal. To control and tune the level of output power, the VAT and PA are placed in between the PN-sequence generator and the transmitter antenna [14].

3.1.3. Receiver

After the signal has reached the receiving antenna, the signal goes through a LNA. To sample the UWB-signal, the ADC must cooperate with a T/H because commercially available ADCs bandwidth are not adequate for the signal of interest. In the end of the chain, a FPGA is used to store the samples acquired by the ADC [14].

3.1.4. Clock generation system

The clock generation system consists of a fractional PLL and a clock distributor. The purpose of using the PLL is to synthesize a frequency f_f from the reference clock, with frequency f_b, generated by the PN-sequence generator. The clock distributor divides the clock-signal, f_b, and introduces an arbitrary phase-shift between both output clock-signals, f_f. This means that both the ADC and T/H are triggered with the clock frequency f_f, but with different phases [14].

3.1.5. Personal Computer

The data is transferred from the measurement hardware through USB-interface to a personal computer (PC). The PC is used to store measurements and process the data. The operating system running on the PC is Windows® 7.

3.2. Transmitted signal: Pseudo random noise sequences

The system presented in Figure 2 is used for detection of vital signs. This includes the signals generated by the system transmitter. A pseudo-random binary sequence generator generates PN-sequences instead of conventional pulse-trains. It has been claimed that the PN sequence is more effective than pulsed system due to higher average power. Higher average power of the signal results in a higher SNR [14].

The PN-sequence generated by the PN-sequence generator is a so-called M-sequence: maximal-length pseudo-random binary sequence. Figure 3 visualizes a binary PN-sequence; it is a sequence of random bits where the binary values correspond to a voltage level. The PN-sequence in Figure 3 was recorded when the output of the transmitter was directly connected to the input of the receiver with a cable. The bit-sequence is generated with a shift-register within $2^m - 1$ clock cycles where m is the length of the shift-register and the clock has a frequency f_b [15]. The repetition rate of the PN-sequence is therefore:

$$f_r = \frac{f_b}{2^m - 1} \quad (4)$$

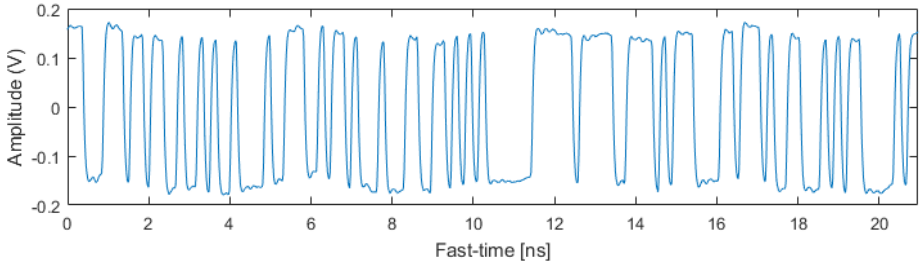

Figure 3: Plot of a single period of an m=7 M-sequence with a clock rate $f_b = 6GHz$.

However, when the PN-sequence is transmitted between the antennas, many frequency components of the PN-sequence are suppressed. This is caused by the bandwidth of the antennas. Compared to the bandwidth of the antennas (section 3.1.1), the bandwidth of the UWB signal generated by the system stretches from a couple of hundred Megahertz up to 3 GHz [15]. It results in a recorded signal presented in Figure 4. Note that the time axis of a single waveform is referred to as fast-time.

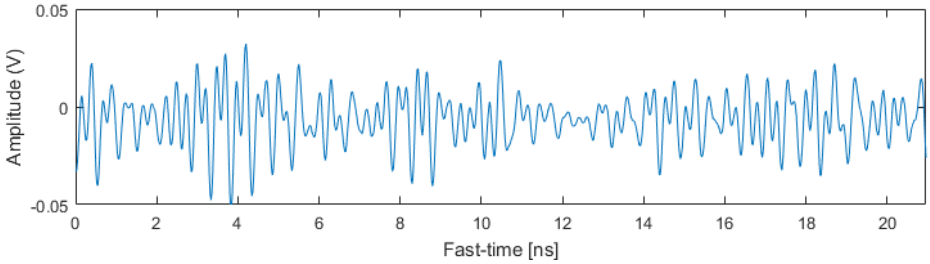

Figure 4. Signal acquired by the receiver of the measurement system.

3.3. Received signal: sampling in fast-time and slow-time

3.3.1. Sampling in fast-time: Synchronous equivalent-time sampling

Since the bandwidth of the transmitted signal stretches up to 3 GHz, the sampling rate of the receiver must be higher than 6 GSa/s in order to sample the signal in real-time, according to Nyquist sampling criteria. However, the T/H-ADC assembly is not capable of such high sampling rates. Consequently, an equivalent sampling method has been employed as a solution to the problem. The idea of the method is to sample a periodical signal (cyclically transmitted PN-sequence) in different positions for every cycle, until one period is reconstructed (Figure 5). For a simple implementation, only one sample is taken per period. The figures in section 3.2 present waveforms with the length of one period where the time axis of the figures is referred to as "Fast-time". Since the PN-sequence is continuously repeated, the fast-time sampling frequency (f_f) must be lower than the repetition rate of the PN-sequence (f_r) in order meet the requirement of the method [14]. The equivalent sampling frequency (f_{eqs}) corresponds to a sampling frequency that would allow reconstruction of one waveform within the in the time frame of one PN-sequence. f_{eqs} can be determined from the following equations:

$$f_{eqs} = \frac{1}{\mathrm{T_{eqs}}} \qquad (5)$$

$$\mathrm{T_{eqs}} = \frac{1}{f_f} - \frac{1}{f_r} \qquad (6)$$

The value of f_f can be derived once f_{eqs} known, since they are directly dependent of one another. However, the importance of f_{eqs} is described in later section 5.1.2. Note that f_r depends on the parameters of the transmitter and is calculated according to equation (4).

In order to preserve the phase and avoid spectral leakage in measurements, the relationship should be satisfied:

$$f_{eqs} = N_f \cdot f_r \qquad (7)$$

where N_f is the number of samples in one recorded period.
To record one period with equivalent time sampling, the number of PN-sequences is:

$$N_p = N_f + 1 \qquad (8)$$

Figure 5 illustrates the timing diagram using the concept of $N_f = 4$.

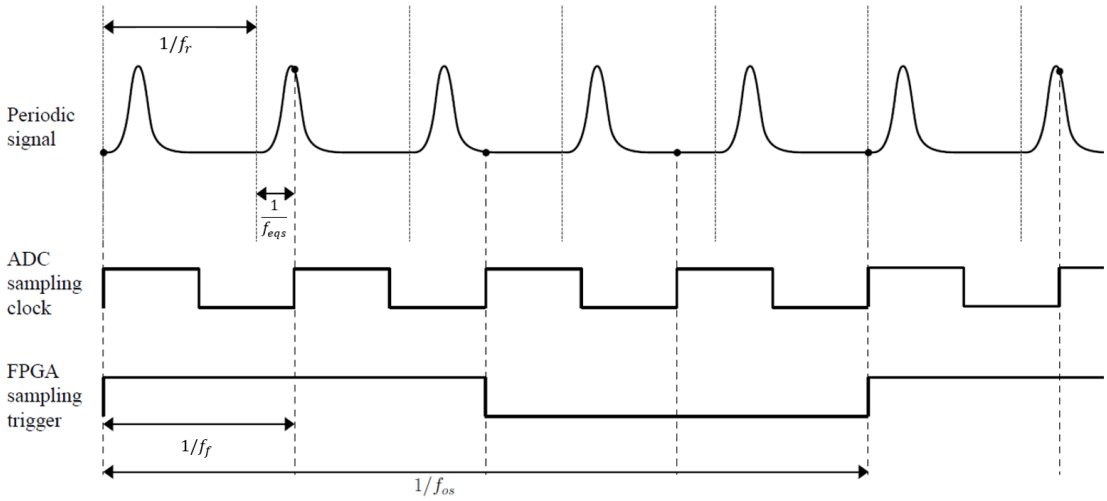

Figure 5. Timing diagram of a synchronous equivalent time sampling system with N_p=5. Black dots in the upper signal indicate samples [15].

In Figure 5 there is something called "FPGA sampling trigger". It indicates the period, $\frac{1}{f_{os}}$, over which the FPGA records all the samples taken by the ADC in order to reconstruct one period.

3.3.2. Sampling in slow-time

Previous section describes the method of recording one waveform as a reconstruction of one PN-sequence. Also, the samples of an individual waveform are represented in a time domain labeled as "Fast-time". The waveforms can be recorded with constant time intervals, T_s, where the theoretical $T_s \geq \frac{1}{f_{os}}$ (see Figure 5). This gives each recorded waveform a unique timestamp in a so-called "Slow-time" domain.

The limit, of how high the slow-time sampling frequency can be, depends purely on how long time it takes for the hardware to record and store one waveform. Even though the ADC is sampling (in fast-time) for every new clock cycle, there is simply no need to save each recorded waveform. According to the Nyquist criteria and the maximal vital sign frequency of 3 Hz (section 2.1). The slow-time sampling frequency ($f_s = 1/T_s$) must be larger than the double maximal frequency, which in this case would be larger than 6 waveforms/s. The higher the slow-time sampling frequency is, the more detailed displacement can be recorded. Yet, if the waveforms are recorded over a longer period of time (in slow-time), a high slow-time sampling frequency would mean increased number of recorded waveforms. Consequently, the total number of recorded samples will be much larger. Hereby, the next limit is the amount of memory available on the hardware to store those samples.

3.4. Principles of operation

The whole process can be described as the function blocks in Figure 6. Starting from the **Transmitter**, a PN-sequence, $p(\tau)$, is repeatedly transmitted towards the **Measurement Object**. The transmitted $p(\tau)$ is reflected by the Measurement Object and recorded by the **Receiver** as $r(\tau)$. The Receiver stores an arbitrary number of $r(\tau)$ in a matrix, $R[m,n]$. When the desired number of $r(\tau)$ has been recorded, the matrix $R[m,n]$ is then transmitted to the **PC**. The PC processes all recorded signals in order to extract the breathing rate, f_{br}, and the heartbeat rate, f_{hbr}.

The synchronization between the Transmitter and Receiver is controlled by the clock of the Transmitter, f_b. However, the clock is distributed to different components of the Receiver by the **Clock Generation System.**

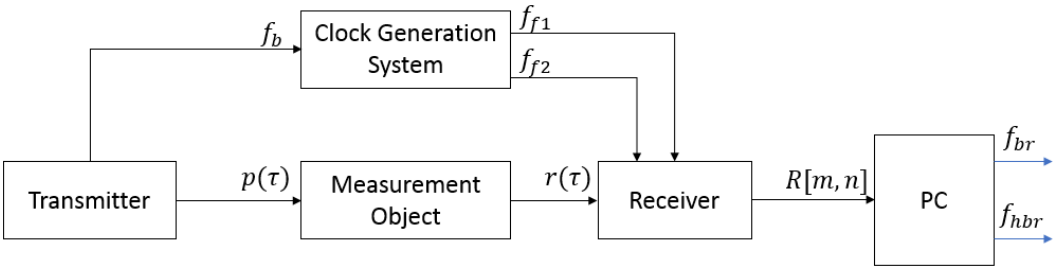

Figure 6. General overview of the measurement system.

3.5. Additional devices

The functionality of the measurement system has been verified throughout the project with two different solutions. Firstly, the ability of the system to detect oscillating displacement generated by a robot. The implementation is described in detail in section 5.2.2. Secondly, in the final stage of the project when attempts to detect the heartbeat rate are made, a reference system for measuring the heartbeat rate is used.

3.5.1. Robot for controlled displacement

A robot setup is built from a set of Lego Mindstorms NXT2.0. The NXT controller unit is programmed in Simulink with blocks "*Simulink Support Package for LEGO MINDSTORMS NXT Hardware*". Lego Mindstorms NXT has been retired by LEGO in 2013. The Simulink support was available until MATLAB R2016b. For this reason, the Simulink support package is not available from MathWorks website [18]. Simulink model is attached in Appendix 2.

3.5.2. Electrocardiogram

Commercially available ECG is used. The model of the ECG is: Plessey PS25003 EPIC Demonstration Kit.

4. Signal processing

4.1. Removal of clutter and DC-component from received signal

A mathematical representation of the received signal, $r(t,\tau)$, can be presented as the sum of the responses of the channel together with the variations caused by the heartbeat and respiration [10]:

$$r(t,\tau) = \sum_i A_i p(\tau - \tau_i) + Ap\big(\tau - \tau_{\mathrm{d}}(t)\big) \qquad (9)$$

To clarify the meaning of the expression, the list of the parameters is explained in following way:

1. $p(t)$ is a transmitted PN-sequence
2. A_i is the amplitude of each multipath component
3. τ_i is the delay of each multipath component
4. A is the amplitude of the signal reflected from the chest
5. $\tau_d(t)$ is the time delay caused by displacement

Each sample of the waveform is recorded at a discrete time instance in fast-time, τ, where N_f is the total number of samples per PN-sequence:

$$\tau = m \cdot T_f \quad \big(m = 1,2,\dots,N_f\big) \qquad (10)$$

where T_f is time interval between each sample in the fast-time domain:

$$T_f = \frac{1}{f_f} \qquad (11)$$

Similarly, each waveform is recorded at a discrete time instance in slow-time, t, where N_s is the total number of waveforms to be recorded [10]:

$$t = n \cdot T_s \quad (n = 1,2,\dots,N_s) \qquad (12)$$

where T_s is the time interval between the timestamps in the slow-time domain at which the waveforms recordings started.
The waveforms are stored in a 2D-matrix, **R** [10]:

$$R[m,n] = r\big(\tau = nT_f, t = mT_s\big) \qquad (13)$$

The recorded waveforms must be pre-processed in order to remove clutter that is mostly caused by the coupling between the antennas. The clutter can be removed by calculating the average waveform and then subtract the average waveform from all recorded waveforms. The method is based on the assumption that all recorded waveforms have a common factor. If the transmitted signal pattern is always the same, and that the antennas have a fixed position in relation to each other, each recorded waveform will contain a multipath component that is nearly identical for all cases: the coupled signal. It leads to a new matrix, X [10]:

$$X[n,m] = x\big(\tau = nT_f, t = mT_s\big) \qquad (14)$$

$$x(t,\tau) = r(t,\tau) - \lim_{T\to\infty}\frac{1}{T}\int_0^T r(t,\tau)dt = Ap\big(\tau - \tau_d(t)\big) - r_0(\tau) \quad (15)$$

$r_0(\tau)$ is the DC-component that is present in the clutter-free waveforms $x(t,\tau)$. To get rid of the DC-component in a waveform, the average value of the waveform is calculated, $x_0(\tau)$, and then subtracted from the clutter-free waveform. The result is saved in a new matrix, Y [10]:

$$Y = y\big(\tau = nT_f, t = mT_s\big) \quad (16)$$

$$y(t,\tau) = x(t,\tau) - x_0(\tau) = Ap\big(\tau - \tau_d(t)\big) \quad (17)$$

4.2. Measure chest displacement with cross-correlation method

Cross-correlation measures the similarity of two signals as a function of the displacement (also known as lag) of one signal relative to the other. Let's denote the compared signals as $g(n+\theta)$ and $h(n+\theta)$ respectively. The definition of cross-correlation for discrete-time signal functions is [19]:

$$C_{gh}(\theta) = \sum_{n=-\infty}^{\infty} g(n)\cdot h(n+\theta) \quad (18)$$

where θ is the lag. Generally, in signal processing, cross-correlation is used to detect a certain signal pattern within a larger recording. The function gives partially an answer whether the small signal $g(n)$ is buried somewhere in $h(n)$ or not. Cross-correlation is commonly applied in detection of radar echoes. Assume that the radar transmits a pulse in an arbitrary direction. The pulse is then reflected from an object and returns to the radar. The radar is recording for a certain time so that the pulse has enough time to return to the radar. However, the pulse constitutes a minor part of the recorded signal and is not obviously detectable because of all noise present in the recorded signal. The problem is solved by cross-correlating $h(n)$(= recorded signal) with $g(n)$ (= original pulse). Highest similarity between the two signals is at the θ that gives the highest value of $C_{gh}(\theta)$ [19]. The lag at the maximal correlation, θ_{match}, indicates the time it has taken for the pulse to reach the object and return to the radar.

In the microwave-based vital sign detection application, a set of signals are recorded by the system as waveforms and then stored in a matrix Y (equation 16). The first waveform, $y(1\cdot T_s,\tau)$, is set as a reference waveform corresponding to $g(n)$ and the cross-correlation is calculated between the first waveform and the whole set of waveforms; $\{y(1\cdot T_s,\tau), y(2\cdot T_s,\tau), \dots, y(N_s\cdot T_s,\tau)\}$.

Unlike in the radar application, θ_{match} corresponds to the shift of the reference waveform caused by the displacement of the chest rather than the distance to the chest. The displacement in distance, $\widehat{vs}(t)$, in relation to the first waveform is:

$$\widehat{vs}(t) = \theta_{match}(t)\cdot\frac{c\cdot T_{eqs}}{2} \quad (19)$$

4.2.1. Displacement reconstructed with cross-correlation method

The frequency bands of the observed vital signs, as mentioned in section 2.1, differ. By applying a band-pass filter to $\widehat{vs}(t)$ with cut-off frequencies of the desired vital sign, all but the important frequency components are going to become suppressed. By implementing the discrete Fourier transform (DFT) to the filtered signal and then calculating the absolute value of the DFT, the frequency spectrum is acquired. The criteria for what is considered as the frequency of a vital sign, is the frequency component with the highest value in the spectrum.

4.3. Measure the chest displacement with point oscillation

Compared to the cross-correlation method, this method is not monitoring the shift of pulse-waveform. Instead, the amplitude of a particular fast time index is monitored over the time of the measurement. In other words: the amplitude changes of an arbitrary sample index, τ, in the waveforms, $y(t,\tau)$, is monitored. Figure 7 shows four waveforms where the three waveforms from top correspond to $y(t,\tau)$ recorded at 3 different occasions: $y(1,\tau), y(2,\tau)$ and $y(3,\tau)$. Only one value is collected from each of the three waveforms with one property in common: the same fast time index $\tau = 200$. The fast-time index is marked with a red vertical line, with a red circle aligned to the line, pointing out the value of the waveform amplitude. Finally, the fourth waveform is a plot of 250 values of $y(t,200)$, where the first 4 values are marked with red dots in the beginning of the fourth plot.

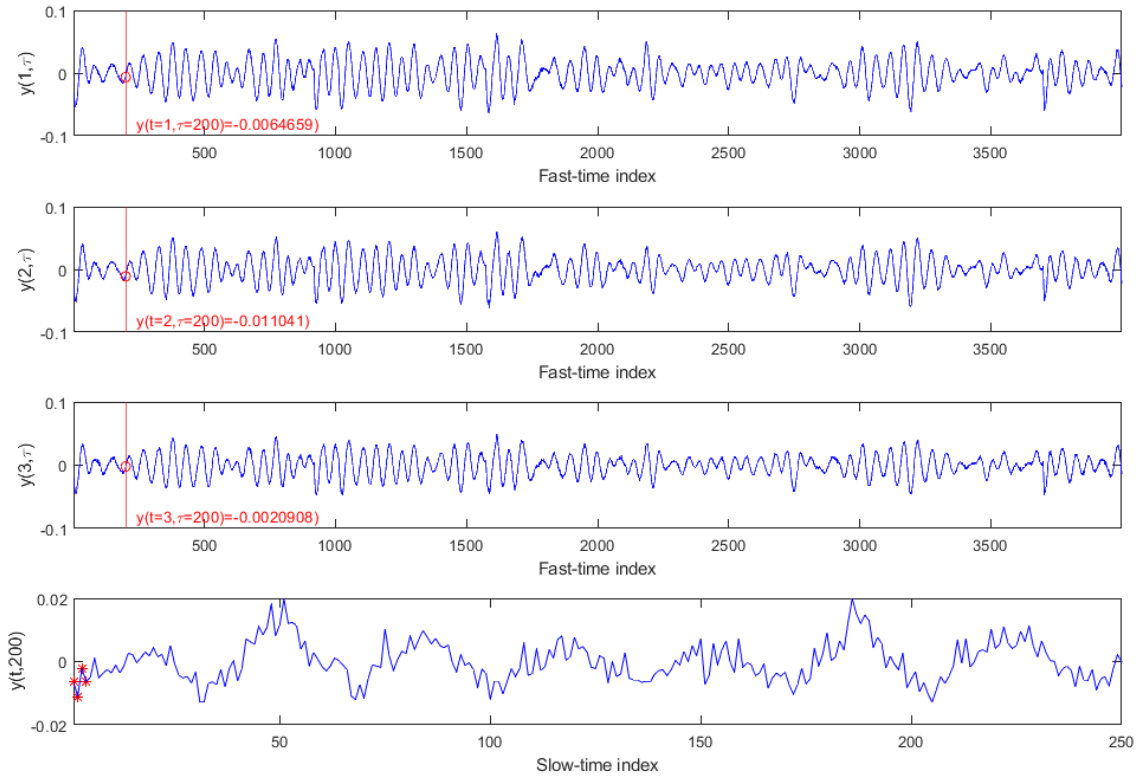

Figure 7. The three waveforms from top are PN-sequences recorded at three different occasions. The fourth plot shows the amplitude of the 200th fast-time index over time.

The fourth plot presented in Figure 7 is in the slow-time domain. By implementing DFT to $y(t,200)$, the oscillation frequency of the sample may be observed. Figure 8

presents the frequency spectrum of the oscillating point. The data used for the demonstration is from an actual measurement where a person was breathing according to the beat of a metronome at 19 BPM, and where the average heartbeat rate was measured with an ECG to 70.24 BPM. In Figure 8, the highest peak of the spectrum is almost aligning with the frequency of the breathing rate. However, there is no peak around the measured heartbeat rate.

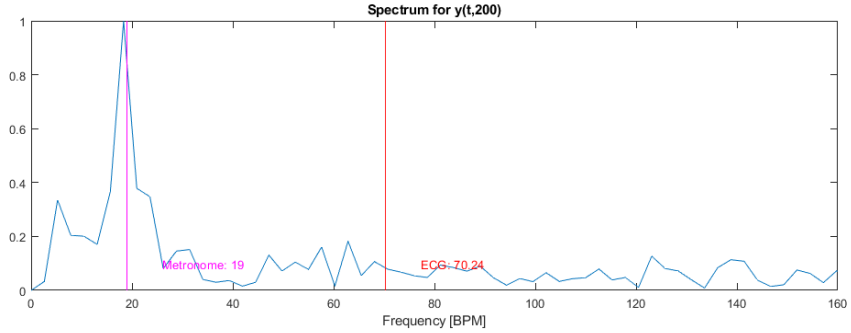

Figure 8. Frequency spectrum of on oscillating point. Data is taken from a measurement where subject was breathing to the beat of a metronome at 19 BPM. An ECG measured average heartbeat rate of 70.24 BPM throughout the measurement.

Moreover, if the environment would be static and noise-free, the measured amplitude at that sample would remain constant. Together with chest displacement, the waveforms obviously shift and the samples at $y(i \cdot T_s, \tau)$, where $i = \{1, \dots, N_s\}$, will oscillate. The advantage using this method, rather than the cross-correlation method, is the fact that it is independent of the fast-time resolution, described in section 5.1.2.

4.3.1. Vital sign detection with point oscillation method

The oscillation of a certain fast-time index, throughout several measured waveforms, is considered as one measured signal. By calculating the absolute value of the DFT of the signal, a frequency spectrum is acquired.

The maximal number of frequency spectrums in a measurement is the same as the number of points in a waveform, N_f. The advantage of calculating all possible frequency spectrums is the fact that each oscillating point can be affected by random noise. An average frequency spectrum improves the result by emphasizing the frequency components of e.g. the vital signs. Furthermore, an average frequency spectrum will suppress the frequency components generated by random noise. To generate an average frequency spectrum, all spectrums must be normalized first. Then, the average spectrum can be calculated by dividing the sum of all normalized spectrums with N_f. Figure 9 presents four frequency spectrums, where the spectrum in the bottom right is an average of 3999 spectrums. In the average spectrum, there is an obvious peak at the frequency of the heartbeat rate.

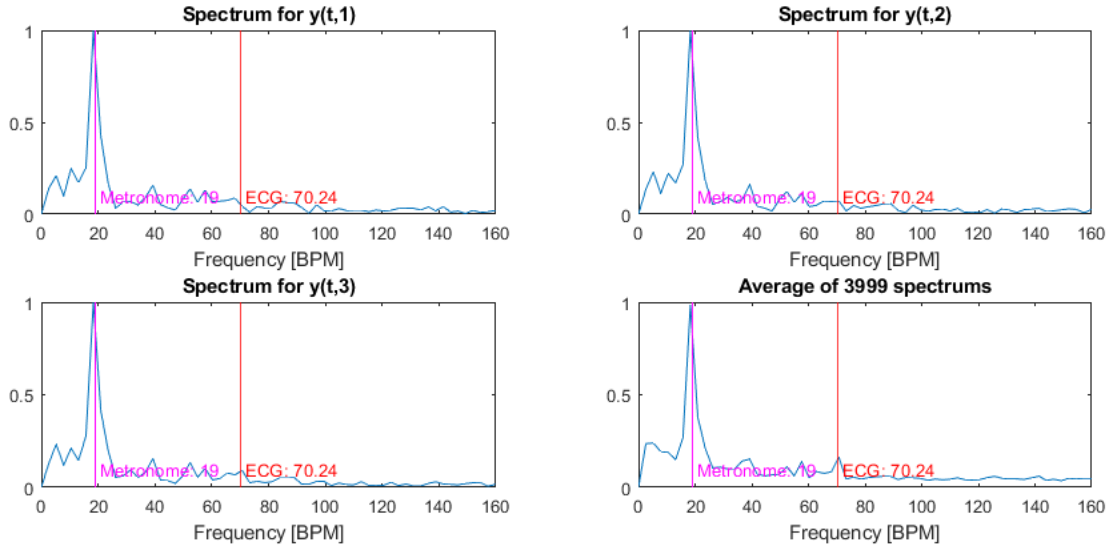

Figure 9. Four frequency spectrums are presented, where the heartbeat rate is only obvious in the average of all frequency spectrums.

4.4. Bandpass filtering

The purpose of bandpass filters is to suppress frequencies outside of the interesting frequency band. Since the frequency bands of heartbeat rate and breathing rate do not overlap, a bandpass filter for each of the vital signs can be designed separately. Thus, when analyzing the filtered signal, irrelevant frequency components will have less influence than before, since they have been suppressed.

The frequency range of each vital sign is mentioned in section 2.1, which is a reference used to decide the cutoff frequencies of the bandpass filters for this project. Furthermore, the filter-type chosen for this task is the Butterworth filter due to the flat frequency response in the passband.

4.5. Harmonics and Notch filters

In previous studies it has been proven that calculating the Fourier transform in slow-time will give a discrete spectrum consisting of several delta functions [10]. These functions are centered at frequencies of the harmonics of f_{br}, f_{hbr} and the intermodulation products of f_{br} and f_{hbr}. Harmonics are integer multiples of a frequency. Given that the frequency band of f_{br} is below the frequency band of f_{hbr}, the harmonics of f_{br} will most likely appear in the frequency band of f_{hbr}. If the breathing is strong, the harmonics may be strong as well. As a consequence of that, the frequency component of the heartbeat rate might be masked by the breathing harmonics. The purpose of a Notch-filter is to suppress a specific frequency component. Since the harmonics appear in the multiples of f_{br}, several Notch-filters must be designed during the signal processing to remove the multiples of the detected f_{br}.

The digital notch-filters used in this project were designed to be 12^{th}-order bandstop IIR filters with a bandwidth of 0.01Hz (corresponding to 0.6 BPM).

4.6 ECG as reference measurement system

The respiration rate can be controlled by the subject directly, however the heartbeat rate cannot. It is necessary to record the heartbeat rate in a trustworthy way to know the true heartbeat rate of the subject throughout a measurement session. A commercial ECG, Plessey PS25003 EPIC Demonstration Kit, is used in the project for this purpose.

The calculation of the average heartbeat rate throughout one session is what is measured in this case. By finding the peaks of the R-waves in the ECG signal, and the time instance at which they were recorded, t_R, the average hearbeat rate is calculated with the following equation:

$$Average\ heartbeat\ rate = \frac{\sum_{i=2}^{N} \frac{60}{t_R(i) - t_R(i-1)}}{N-1} \qquad (20)$$

where N is the total number of peaks of the appearing R-waves. In Figure 10, the peaks of the R-waves are marked with red stars:

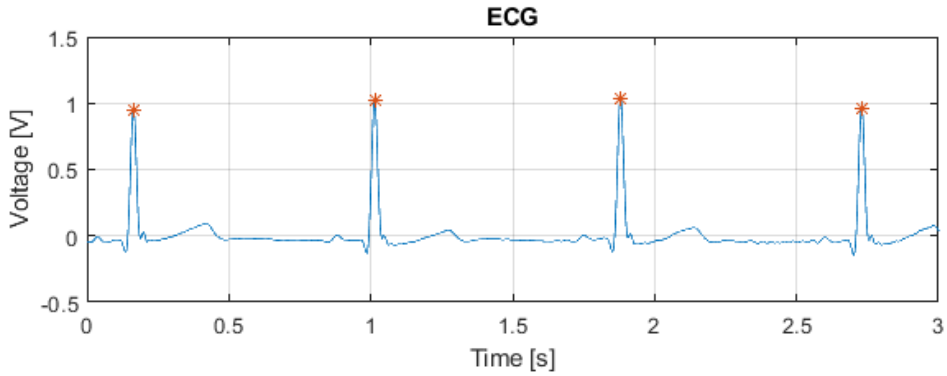

Figure 10. Recorded ECG data that has been marked with a red star on each R-wave peak

5. Measurements and Results

5.1. Practical issues

5.1.1. Delay implementation between waveforms

Without knowing the waveform recording rate, f_s, it is not possible to know the interval between the time stamps of the recorded waveforms in the slow-time domain. Thus, it is not possible to retrieve the frequency spectrum of the displacement. What was not considered in the initial receiver software design was the rate at which the waveforms should be recorded. This feature had to be implemented as a part of the project. After examining the program for both the FPGA and the PC it was noted that once the FPGA recorded a waveform it was directly transmitted to the PC and the PC would save this waveform in a file. Next waveform was going to be recorded once the waveform was saved in a file. However, the recording-and-transmission time was approximately 1 second in total but could vary over time. Figure 11 is a screenshot of an oscilloscope measuring the repetitive recording of waveforms. By studying Figure 11 it is known that the recording of the waveform takes just a couple of milliseconds. The conclusion is that the bottleneck of the waveform recording rate was the transmission of the waveform data from the FPGA to the PC.

Figure 11. Picture of oscilloscope measuring period time of the digital output on the FPGA. Output is set to high when the delay is running and low when the FPGA is recording a waveform.

To bypass the transmission-time bottleneck, the problem is solved by recording a desired number of waveforms with a certain recording rate and when done, all the recorded waveforms will be transmitted in one sequence to the PC.

A way to determine the recording rate is by introducing a certain delay between recordings and monitor the recording rate somehow. In this case there is no built-in delay function that could solve the problem. Instead the delay is introduced by iteratively executing a set of operations. In this case, one time-consuming operation is changing the state of a digital output on the FPGA board. The delay works in such way that the output is set to high in all iterations (even if it is not changing the state of the output), and once the iterations are finished, the output is set to low and the FPGA-

board starts recording the waveform. In Figure 11, the waveforms are recorded with 20ms intervals giving a slow-time sampling rate:

$$T_s = 20ms \quad (21)$$

$$f_s = \frac{1}{T_s} = \frac{1}{20ms} = 50\ samples/s \quad (22)$$

Normally, the frequency of the vital signs does not exceed 3Hz. To meet the Nyquist sampling theorem, it is more than sufficient to have a system with f_s = 50 samples/s for measuring the chest displacement. This means that it is not necessary with such high sampling rate.

Nevertheless, a large number of samples improves the resolution of the frequency spectrum. Consequently, a more accurate frequency estimation of the vital signs is possible. To gather many samples with low f_s requires a longer duration of the measurement. A high f_s does not require the measurement to be carried out for a long period. However, a high f_s makes it difficult to design digital filters for lower frequencies, where the vital signs belong. It is therefore necessary to make a trade-off.

To adjust f_s, the digital output on the FPGA is continuously measured and the time interval between recorded waveforms is easy to monitor. Finally, the delay is adjusted by changing the number of iterations. The block diagram of the FPGA-program is attached in Appendix 1.

5.1.2. Resolution problem for cross-correlation method

As mentioned in section 2.2, when PN-sequences are transmitted towards an object, they are reflected from the object and then recorded by the receiver. The received signals should look the same if the object is constantly static. However, if the object moves, the time that it takes for a PN-sequence to return to the receiver will change: it will return quicker to the receiver if the object moves towards the antenna constellation, but it will take longer time to return to the receiver if the object moves away from the antennas. This will result in a time shift of the recorded waveform. Assume that there is no noise in the received signals and that the medium doesn't cause power loss. The only difference between the shifted and non-shifted signal will be a sample rotation, like in Figure 12.

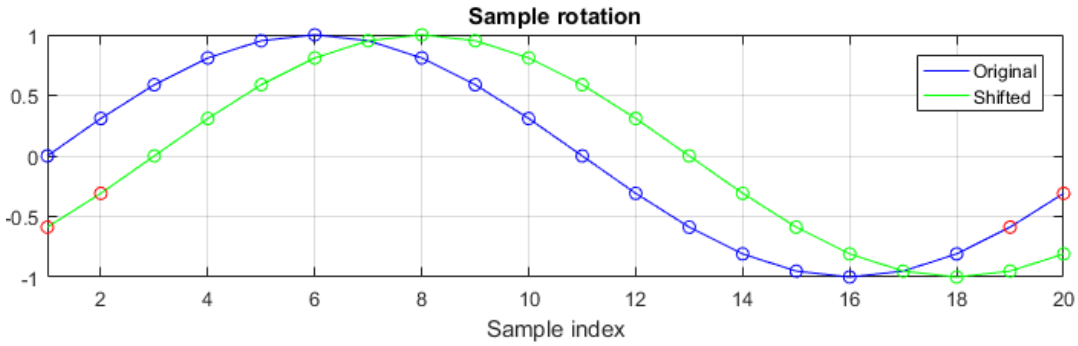

Figure 12. Two last samples of the blue waveform are marked as red circles. Rotating the blue waveform with two samples results with the green waveform. The first two samples of the green waveform correspond to the last two samples of the blue waveform.

Using cross-correlation to detect the distance and direction of the shift (referred to as 'lag') between recorded signals is highly dependent on the f_{eqs}. The higher the f_{eqs} is, the smaller shifts can be detected. On the other hand, a high f_{eqs} requires the hardware to record more points per waveform, N_f. If d_{min} is the smallest desired displacement to be detected, then:

$$\mathrm{f_{eqs}} = \frac{c}{2d_{min}} \qquad (23)$$

where c is the speed of light. The propagation speed of the transmitted signals is assumed to be equal to c. The following relation should be aimed for:

$$N_f \cdot f_r \geq f_{eqs} \qquad (24)$$

since N_f is an integer and that f_r is a fixed parameter, the value of N_f must be large enough to satisfy the relation in equation (24). It is necessary to consider N_f since the measurement hardware has a limited amount of memory. The higher N_f is, the higher amount of memory is used for each recorded waveform.

As a demonstration of the problem, a simulated case has been carried out where the f_{eqs} has been set to 30 GSa/s. By deriving from equation (23), the smallest detectable displacement with such sampling frequency is:

$$d_{min} = \frac{c}{2 \cdot f_{eqs}} = \frac{299792458\ m/s}{2 \cdot 3 \cdot 10^{10} Hz} \approx 0{,}005m = 5mm \qquad (25)$$

which is also seen in the plot from the simulated reconstruction in Figure 13. The pink plot is a simulation of a sinusoidal displacement. Simulated PN-sequences were then shifted according to the displacement magnitude of the pink plot. Finally, reconstructing the displacement with cross-correlation method gave the blue plot as output. It is evident that the resolution is insufficient to detect small changes. The magnitude of displacement that is caused by the heartbeat is much lower than 5 mm, thus an even higher f_{eqs} is needed.

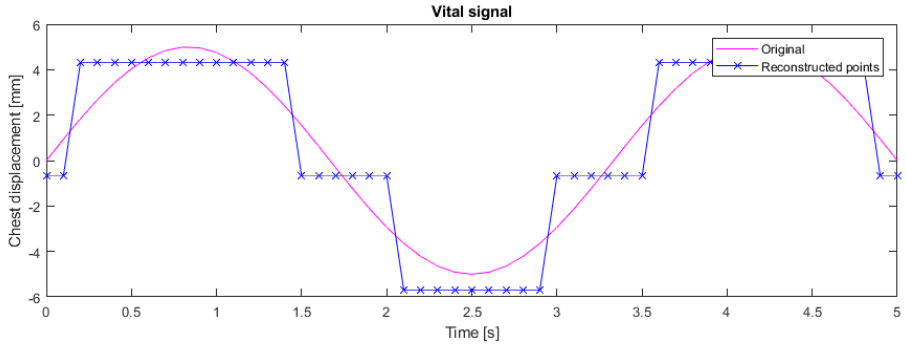

Figure 13. A demonstration of the influence that fast-time resolution has on the performance of the displacement reconstruction with cross-correlation method.

By defining $d_{min} = 0.8mm$, which is significantly smaller than the previous value, a new f_{eqs} can be calculated by first calculating the minimal number of samples per waveform N_f:

$$d_{min} = \frac{c}{2 \cdot f_{eqs}} = \frac{c}{2 \cdot f_r \cdot N_f} \quad (26)$$

$$\rightarrow N_f = \frac{c}{2 \cdot f_r \cdot d_{min}} = \frac{299792458}{2 \cdot \frac{6 \cdot 10^9}{2^7 - 1} \cdot 0.8 \cdot 10^{-3}} \approx 3966 \quad (27)$$

Making N_f even larger will improve the sensitivity of displacement, therefore the value is slightly increased to:

$$N_f = 3999 \quad (28)$$

giving following:

$$f_{eqs} = N_f \cdot f_r = 3999 \cdot \frac{6 \cdot 10^9}{2^7 - 1} \approx 188.93\ GSa/s \quad (29)$$

The reconstruction using the latest parameters is presented in Figure 14 below:

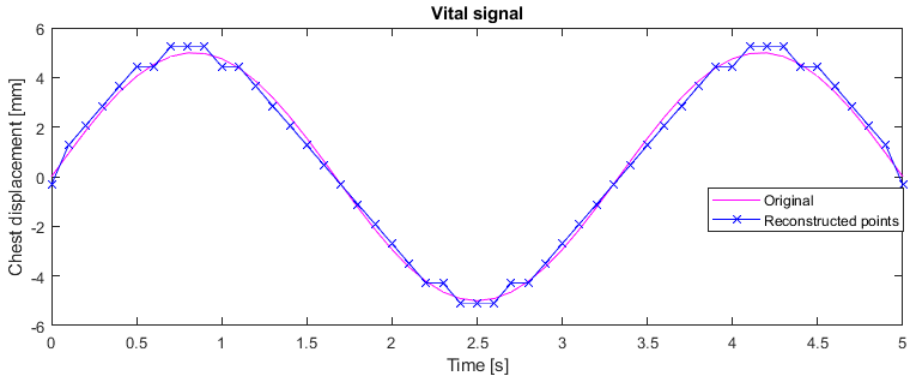

Figure 14. The reconstructed displacement aligns better with the originally simulated displacement, due to higher f_{eqs}.

5.2. Measurements and results

5.2.1. Simulation

The main purpose of simulation is to test and verify the signal processing methods. In addition, measurement parameters, such as sampling frequency, can also be determined through simulations.

This can be considered as a controlled environment where arbitrary magnitudes and frequencies of the breathing rate and heartbeat rate are set by the user. The only considered method in the simulation was the cross-correlation method because the oscillating-point method was not considered until later state of the project.

The simulation starts by simply generating the artificial chest displacement, which is in the slow-time domain (based on equation (1)). The simulated chest displacement is presented in Figure 15 as a pink waveform. Note that the amplitude is exaggerated and that three unique samples of the chest displacement are marked in the plot.

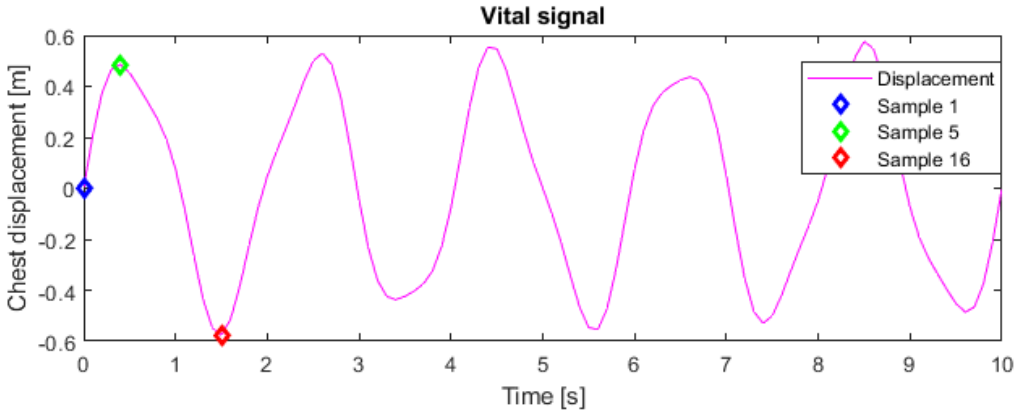

Figure 15. Simulated chest displacement in slow-time domain. The diamonds indicate a displacement value of a certain sample.

Next, a matrix of triangular pulse-sequences is generated. The reason for using triangular pulse sequences instead for PN-sequences here is purely to simplify the demonstration. Figure 16 illustrates three of the sequences from the matrix. Each sequence is identical since they correspond to periodic signal transmission.

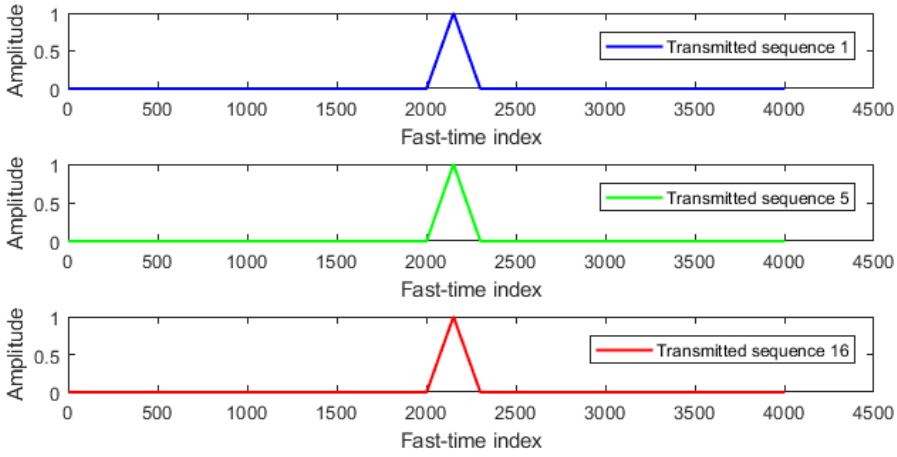

Figure 16. Transmitted signal is always the same. Three of the transmitted signals are presented in the figure.

Observe Figure 15 and Figure 16. The colors of the points in Figure 15 match with the colors of the pulse sequences in Figure 16. The relationship is that the time instances of the points in Figure 15 correspond to the time at which each pulse sequence from Figure 16 is going to be transmitted. The amplitude of the points will shift each individual pulse sequence according to equation (2) and (3). Figure 17 presents the recorded echoes of the three transmitted sequences. The sequences are clearly shifted because they were reflected of the chest at different distances.

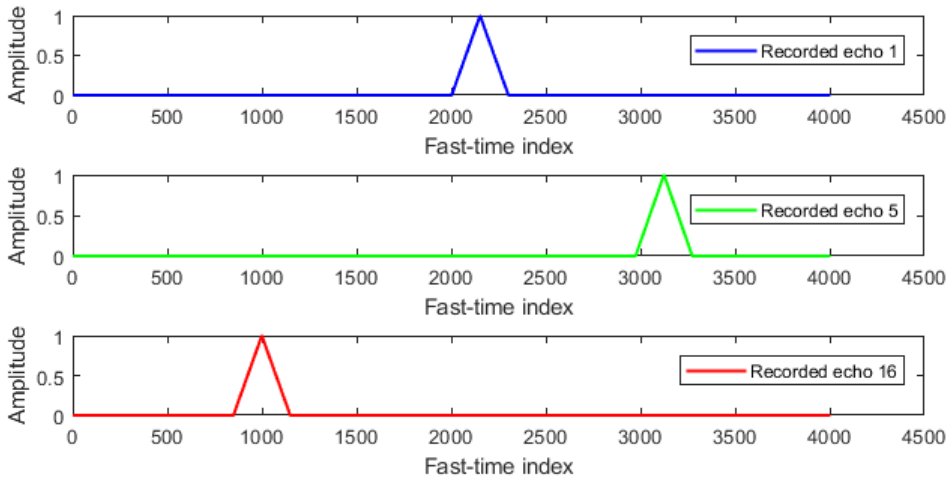

Figure 17. The transmitted signals from Figure 16 have been reflected from the chest at different distances.

Now, if all echoes are calculated and stored in a matrix, the matrix can be illustrated as a 2D image, presented in Figure 18. Each column in the image corresponds to one recorded echo. The darker the color, the lower is the value of the pulse waveform. Similarities can be seen between Figure 15 and Figure 18. However, there is one step left to reconstruct the displacement.

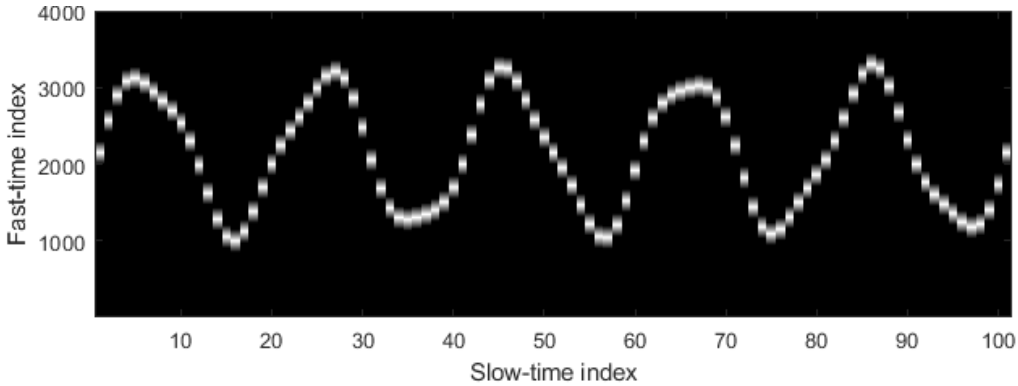

Figure 18. All shifted pulse echoes displayed in a 2D image, where each column corresponds to the pulse echo.

The basic idea of the cross-correlation method is to use one pulse sequence as reference fast-time index waveform. Then, cross-correlation is performed between the reference waveform and every single shifted pulse separately as instructed in section 4.2 . What is important in this method is to know the lags at which the correlations are computed. The lag at which the correlation is the highest indicates the current distance between

the reference position and the subject. If the lag is changing in time, a movement of the subject is detected.
Figure 19 shows two plots on top of each other. The pink line is the original simulation of the displacement. The blue crosses correspond to displacement points reconstructed from the shifted pulse echoes.

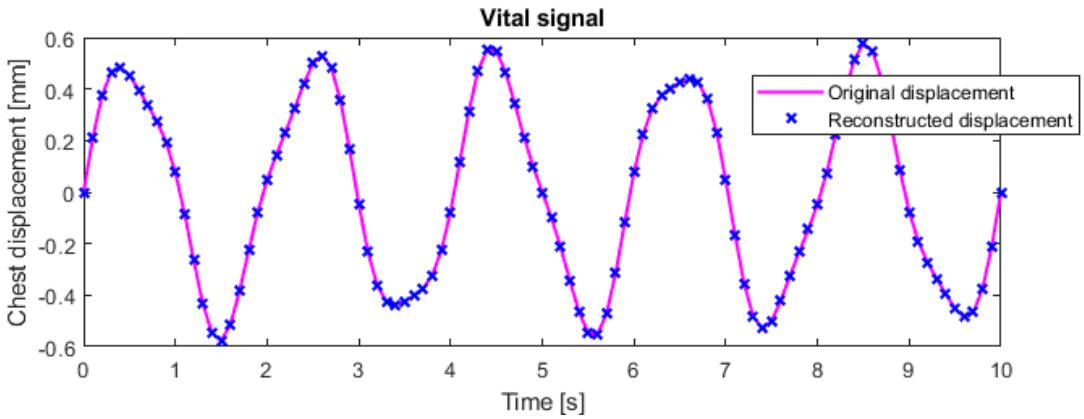

Figure 19. Reconstructed displacement compared to the original displacement.

The frequency spectrum of the original- and reconstructed displacement are presented in Figure 20.

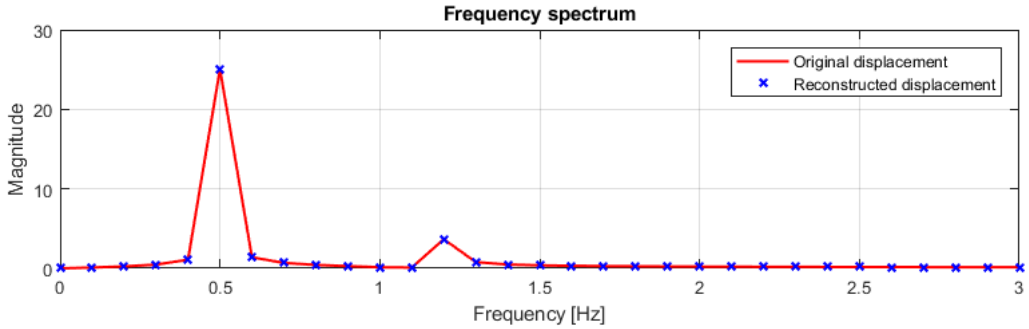

Figure 20. Frequency spectrum of the reconstructed displacement compared to the frequency spectrum of the original displacement.

As mentioned in section 5.1.2; lower amplitudes of the chest displacement are more challenging to reconstruct due to higher requirements on the fast-time resolution. By modifying amplitude parameters of the simulated chest displacement into more realistic values, a sufficient equivalent sampling frequency f_{eqs} can be estimated. The estimation can be made by calculating a new f_{eqs} according to equations from section 5.1.2. Figure 21 presents the frequency spectrum of the simulated chest-displacement with the chest-displacement specifications:

- Respiration amplitude: 5mm
- Respiration frequency: 0.5Hz
- Heartbeat amplitude: 0.08mm
- Heartbeat frequency: 1.2Hz

where $f_{eqs} = 150\ GSa/s$.

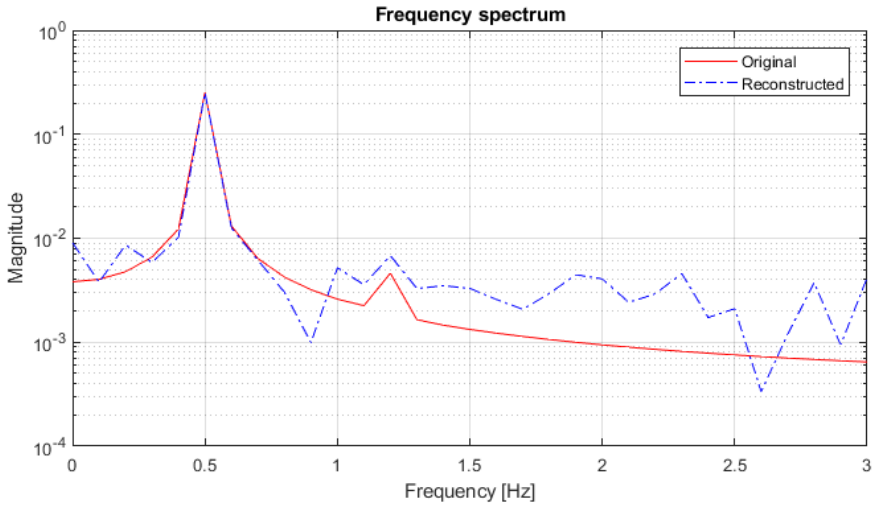

Figure 21. Frequency spectrum of the reconstructed displacement compared to the frequency spectrum of the original displacement in a semilogarithmic plot.

The repetition rate of the PN-sequences is calculated using equation (4) and properties described in the description of Figure 3:

$$f_r = \frac{f_b}{2^m - 1} = \frac{6GHz}{2^7 - 1} \approx 47.2\ MHz \quad (30)$$

As seen in Figure 21, sufficient fast-time resolution is used since the frequency component of the heartbeat rate (peak at 1.2 Hz) is visible in the frequency spectrum of the reconstructed chest displacement. Minimal number of sample points per recorded waveform, N_f, can be calculated by rewriting equation (7):

$$N_f = \frac{f_{eqs}}{f_r} = 3175 \quad (31)$$

5.2.2. Robot for controlled displacement

Before trying to measure the breathing- and heartbeat rate of a person, the measurement system was verified by measuring a controlled displacement. This displacement has much higher amplitudes than what the vital signs generate. The setup for generation of controlled displacement is seen in Figure 22. It is a robot setup that is programmed to move a plate back and forth with an arbitrary frequency set by the user. The robot setup consists of 4 parts:

1. controller unit
2. electrical motor
3. a platform ensuring horizontal movement
4. metal plate

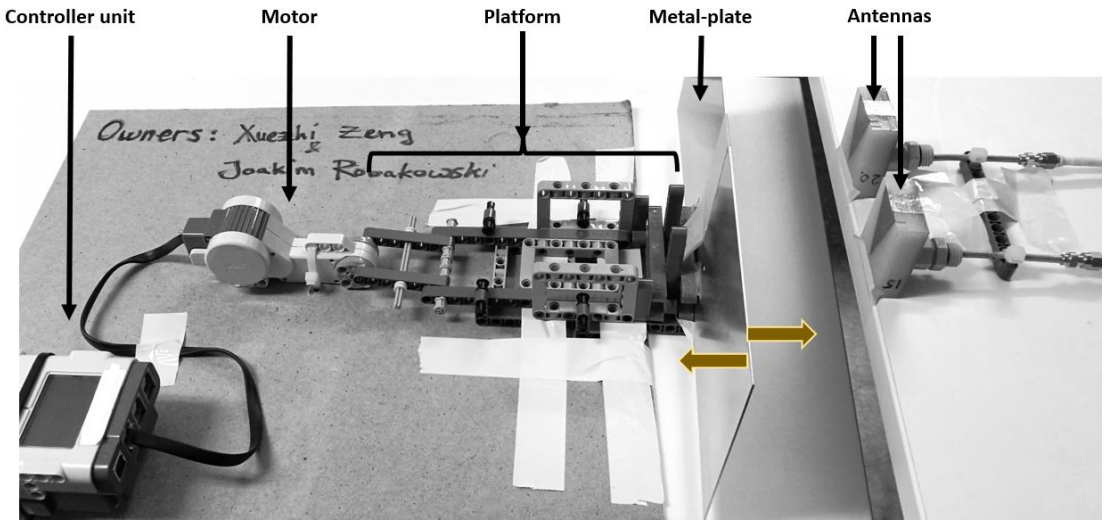

Figure 22. Robot platform facing the antennas. The dark yellow arrows on the metal plate illustrate the directions of the metal-plate movement.

The motor can move the metal-plate back and forth with frequencies between 8-160 BPM, which is within the typical frequency range of the two vital signs. However, the displacement amplitude of the robot setup is $\pm$7.5mm which is a bit larger than the typical chest displacement caused by respiration ($\pm$5mm). Figure 23 shows a close-up image of the motor.

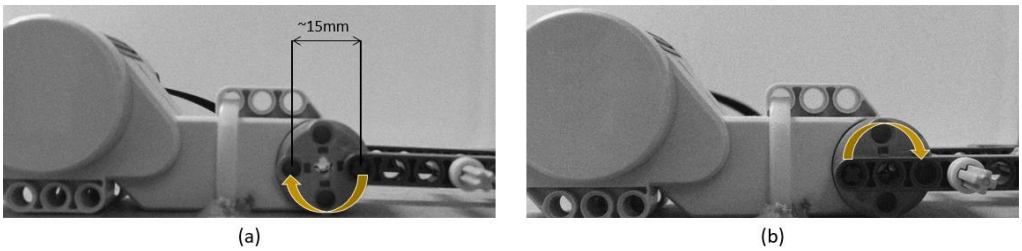

Figure 23. Electrical motor: Yellow arrows in (a) and (b) illustrate the rotor movement. (a) also shows the approximate diameter of the rotor, which corresponds to the range of displacement of the metal plate.

The plates that are attached at the end of the robot arm serve the purpose of reflecting the UWB PN-sequences. The reflectance of materials may vary and metals in general are better at reflecting high frequency electromagnetic signals than wood or skin. Displacement with the robot setup was tested with both a metal plate and wooden plate.

The real measurement system was initially tested in a controlled environment where a moving object was controlled by a robot setup in two different ways: when the robot was set to move a metal plate with high- respectively low frequency.

Using the measurement data gathered from measurements performed on the robot setup, the signal processing methods can be verified since it is known what to be expected in the frequency domain. Unlike the simulated case, the recorded signal has to be preprocessed before reconstruction due to e.g. clutter, as described in section 4.1.

Both methods, mentioned in sections 4.2 and 4.3, were able to detect the frequencies of the displacement frequency very well. Figure 24 and Figure 25 show the results obtained with the cross-correlation method. In Figure 24 and Figure 25, it is clear that the displacement distance is not accurately estimated since the robot-setup is moving the metal plate back and forth within the range of 15 mm. The reason for this behavior is difficult to speculate because the top-to-top range is higher for higher frequencies of the metal plate movement. Nevertheless, the highest peaks in the frequency spectrum

are strongly dominant and occur at an expected frequency instance. Figure 26 and Figure 27 represent the frequency domain of the displacement acquired with the oscillating-point method. Figure 26 and Figure 27 show the highest peaks in the expected frequency instances, but there are noticeable peaks of harmonics in Figure 26. Harmonics are simply frequency components in the signal that are multiples of another frequency. In the case presented in Figure 26 the harmonics are multiples of ~17.76 BPM. The cross-correlation method allows reconstruction of the displacement pattern in time-domain.

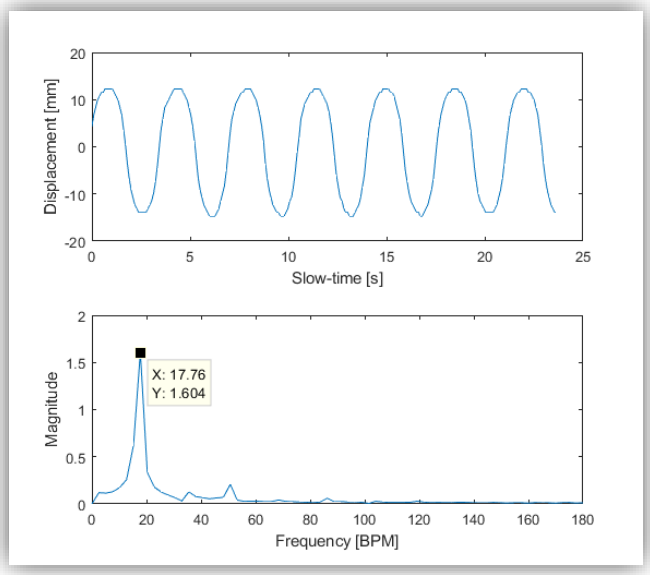

Figure 24. Measurement result acquired with the cross-correlation method from measurement performed on the robot with frequency varying between 16-18 BPM.

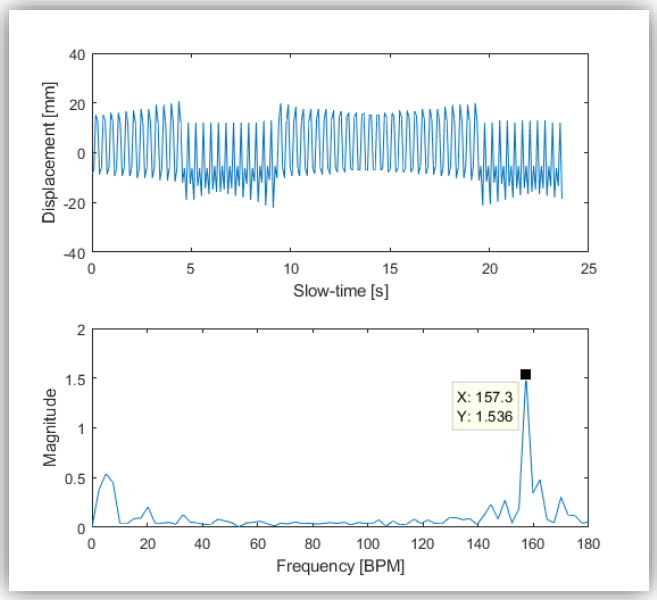

Figure 25 Measurement result acquired with the cross-correlation method from measurement performed on the robot with frequency varying around 158 BPM.

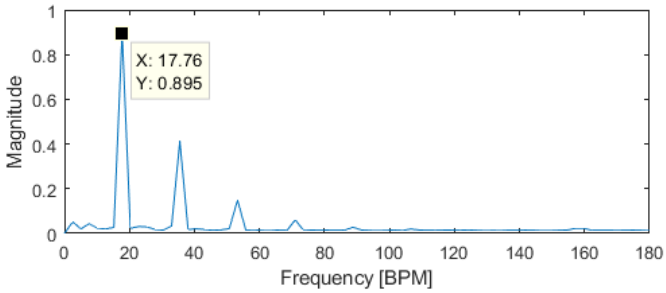

Figure 26. Measurement result acquired with the oscillating point method from measurement performed on the robot with frequency varying between 16-18 BPM. Distance between antennas and metal plate: ~10cm.

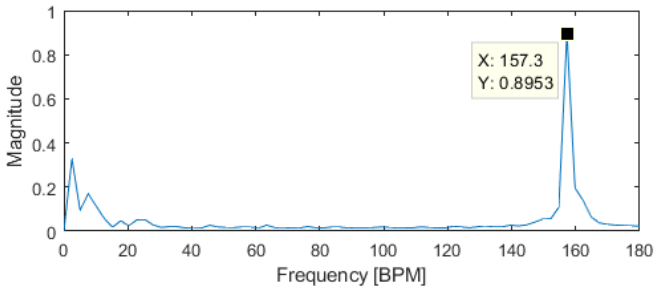

Figure 27. Measurement result acquired with the oscillating point method from measurement performed on the robot with frequency varying around 158 BPM. Distance between antennas and metal plate: ~10cm.

5.2.3. Measuring the respiration only

Once the signal processing methods are verified (using the measurement setup together with the robot setup), it is time to try the vital sign detection: UWB signals reflecting from the chest. A simple way to control the displacement of the chest is by breathing to the rhythm of a metronome. At each beep of the metronome the subject changes from breathing in to breathing out, and vice versa.

Like the robotic setup, the displacement frequency caused by breathing can be controlled. However, there are two key differences that affect the results:

1) the ability to reflect signals by the human compared to the metal plate
2) the amplitude of displacement generated by the mechanical setup and the chest.

Figure 28 shows two graphs with two plots each. Both graphs represent the frequency spectrum of the measured displacement. However, the graphs are divided by the methods used for reconstruction. In many cases, not just as in the one presented in lower graph of Figure 28, the low frequency components tend to be dominant. This phenomenon makes it difficult to determine the breathing rate just by finding the highest peak in the lower frequency spectrum. The unwanted frequency components are removed by filtering the slow-time domain data with a bandpass filter within the breathing frequency band mentioned in section 2.1.

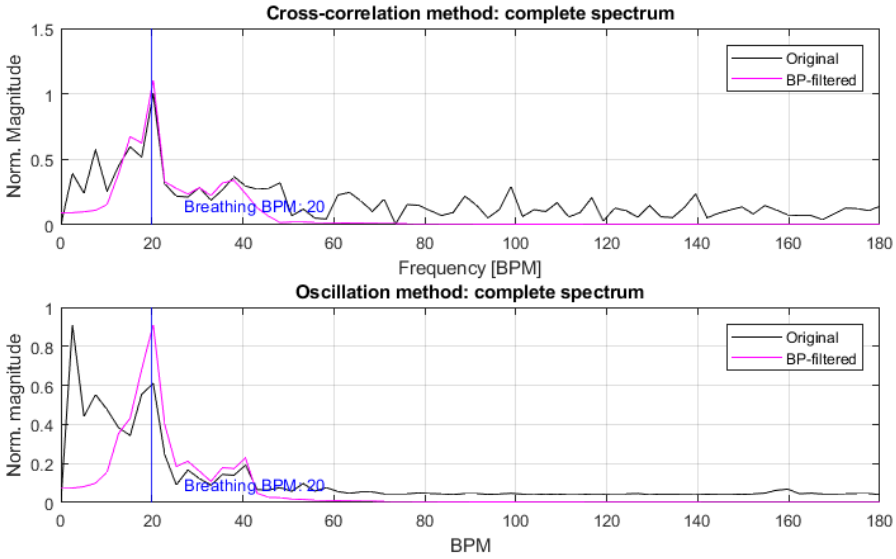

Figure 28. Measurement results acquired when subject was breathing to a metronome set to 20 BPM at 10cm distance, facing the antennas. Vertical blue line indicates the expected frequency.

Figure 29 presents measurement results from a case where the breathing rate was significantly higher than for the case presented in Figure 28. In these figures, it seems that the cross-correlation method works better than the oscillation method. However, Table 2 and Table 3 present all the results from the estimations of breathing rate with both methods. The results show that oscillating-point method is much more reliable than the cross-correlation method.

In total, the percentage of accurate estimations of the respiration frequency was approximately ~67% with cross-correlation method compared to ~90% with the

oscillation method. Average spectrum calculation was applied in the oscillation method.

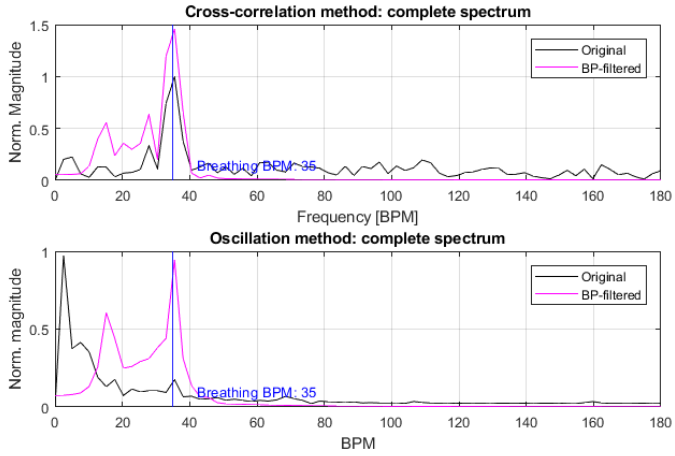

Figure 29. Measurement results acquired when subject was breathing to a metronome set to 35 BPM at 10cm distance, facing the antennas. Vertical blue line indicates the expected frequency.

Table 2. All results from measuring the breathing frequency at different distances with antennas facing the back of the subject.

Respiration, Facing away from antennas	*Corrrect breathing frequency estimations using:*	
Distance	*Cross-correlation method*	*Oscillation method*
0 cm	3 of 6	5 of 6
1-3 cm	3 of 4	4 of 4
5-10 cm	6 of 7	6 of 7
~50 cm	1 of 2	2 of 2
~100 cm	0 of 2	1 of 2
Total:	**13 of 21**	**18 of 21**

Table 3. All results from measuring the breathing frequency at different distances with antennas facing the chest of the subject.

Respiration, Facing antennas	*Corrrect breathing frequency estimations using:*	
Distance	*Cross-correlation method*	*Oscillation method*
0 cm	4 of 5	5 of 5
1-3 cm	2 of 5	2 of 5
5-10 cm	9 of 10	10 of 10
~50 cm	7 of 13	13 of 13
~100 cm	1 of 2	2 of 2
Total:	**23 of 35**	**32 of 35**

5.2.4. Detection of both breathing rate and heartbeat rate

Other studies have shown that the rate of successful detections of vital signs was affected by the position and behavior of the subject [14]. Measurements were therefore performed under different conditions, such as:

- the distance between the subject and antennas
- Whether the antennas face the chest or the back of the subject
- Whether the subject is breathing or not
    - if the subject is breathing then is the subject breathing to the rhythm of a metronome?

These measurements were done in order to investigate which case gives the best detection outcome. Figure 30 shows the subject facing the antennas at a distance of approximately 40 cm.

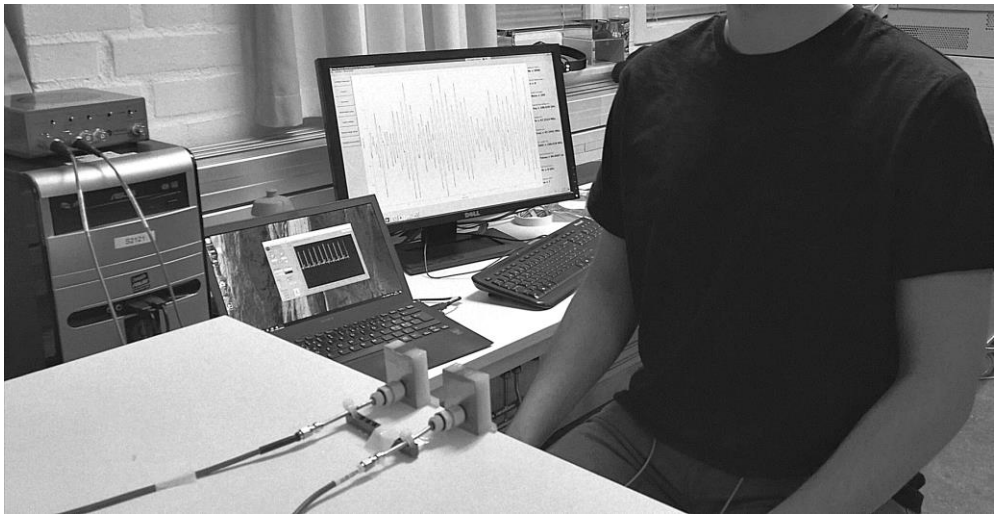

Figure 30. Subject is sitting in front of the antennas that are attached to a table. Laptop is recording ECG data while the desktop PC gathers data from the UWB measurement setup.

Detection of the heartbeat rate was the greatest challenge. The reason is that a heartbeat has a small impact on the body displacement.

By studying Table 4 and Table 5, there are two important conclusions that can be drawn from the experiment:

1) **Oscillation method gives better results.**
   The difference of the two presented signal processing methods is the fact that the cross-correlation method did *not* manage to repetitively detect the heart-beat rate for any of the studied cases. The oscillation method did.
2) **Position: Sit 0-10cm away from antennas, face antennas and hold breath.**
   The case for which the heartbeat rate was detected in every measurement was when the chest of the subject was facing the antennas at a distance of 0-10cm while the subject was holding its breath (Table 5).

Table 4. All results from measuring the vital signs at different distances with antennas facing the back of the subject.

Heart-beat rate, Facing away from antennas	*Corrrect hear-beat frequency estimations using:*			
Distance	*Cross-correlation method*	*Oscillation method*	*Oscillation method using Notch-filters*	*Breathing during measurement*
0 cm	0 of 5	2 of 5		**No**
0 cm	1 of 6	1 of 6	2 of 6	**Yes**
1-3 cm	1 of 5	3 of 5		**No**
1-3 cm	1 of 5	4 of 5	4 of 5	**Yes**
10 cm	0 of 5	2 of 5		**No**
10 cm	0 of 6	3 of 6	3 of 6	**Yes**
~40 cm	2 of 15	4 of 15	4 of 15	**Mixed**
Total:	**5 of 47**	**19 of 47**	**13 of 32**	

Table 5. All results from measuring the vital signs at different distances with antennas facing chest of the subject.

Heart-beat rate, Facing antennas	*Corrrect hear-beat frequency estimations using:*			
Distance	*Cross-correlation method*	*Oscillation method*	*Oscillation method using Notch-filters*	*Breathing during measurement*
0 cm	0 of 5	4 of 5		**No**
0 cm	0 of 7	2 of 7	4 of 7	**Yes**
1-3 cm	1 of 5	3 of 5		**No**
1-3 cm	2 of 5	2 of 5	4 of 5	**Yes**
10 cm	2 of 5	5 of 5		**No**
10 cm	0 of 7	1 of 7	4 of 7	**Yes**
~40 cm	1 of 15	5 of 15	4 of 15	**Mixed**
Total:	**6 of 49**	**22 of 49**	**16 of 34**	

When the subject is breathing, harmonics appear in the multiples of the breathing frequency. The magnitude of the harmonics is often higher than the magnitude of the frequency component of the heartbeat rate. To get rid of the harmonics, notch-filters have been suggested [20]. However, notch-filtering makes significant difference in some cases, both good and bad. Ideally, the notch filters remove the harmonics that appear in the signal, which should emphasize the peak of the true heartbeat rate. An example of successful implementation of both a bandpass-filter and several notch-filters is presented in Figure 31 and Figure 32.

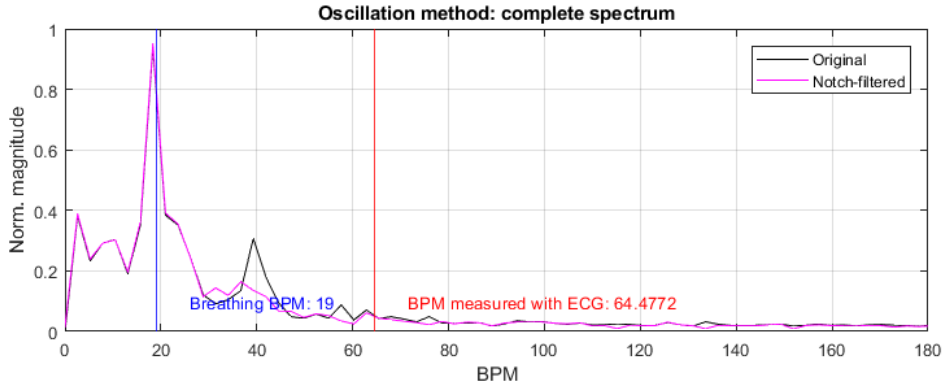

Figure 31. Frequency spectrum of measured displacements. Subject is facing the antennas. Distance to subject: 10cm. Breathing metronome: 19 BPM. Red vertical line indicates the average heartbeat rate measured with ECG

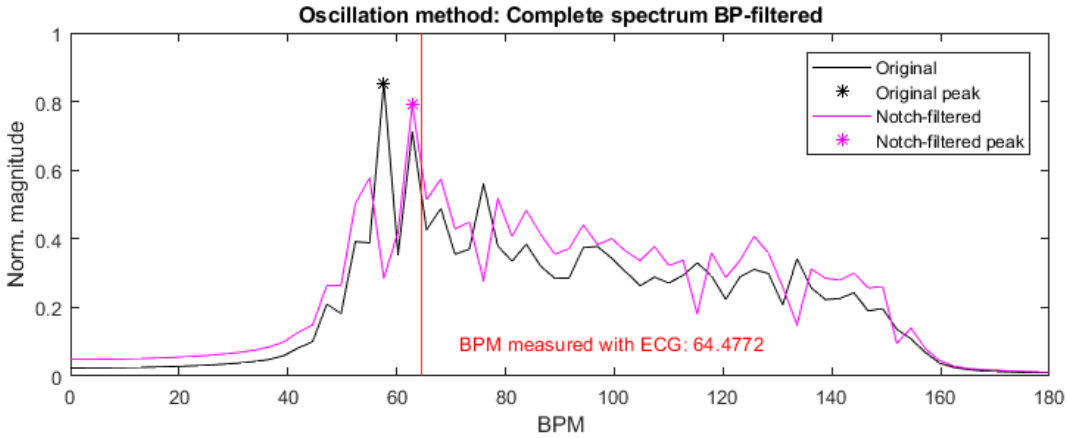

Figure 32. Spectrum of bandpass filtered signals from the same measurement as described under Figure 31.

On the other hand, the harmonics might appear close to the heartbeat rate. Notch-filters, created to remove the specific harmonics, might also suppress the frequency component of the heartbeat rate. Thereby, leading to erroneous estimation of the vital sign frequency. An example taken from the performed measurements is presented in Figure 33.

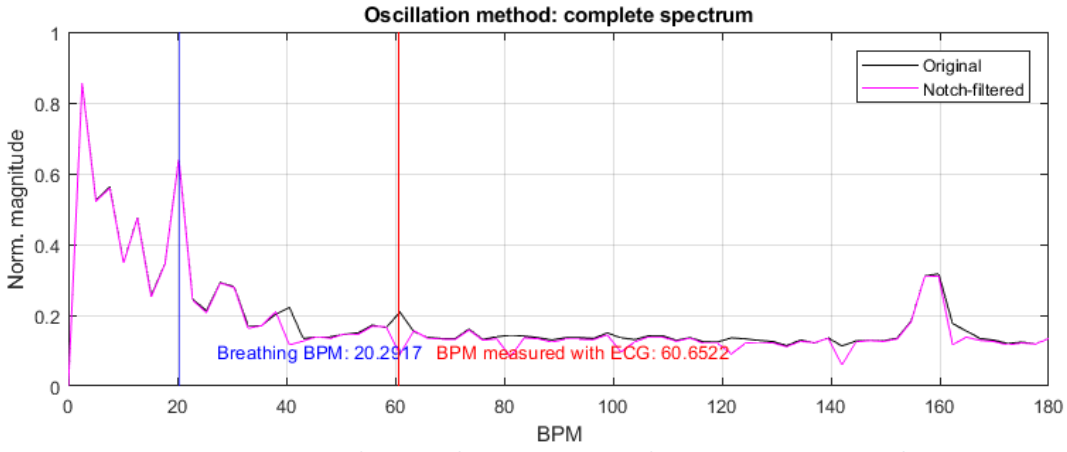

Figure 33. Frequency spectrum before and after applying notch-filters. Second harmonic of the breathing rate appears near the heartbeat rate. Notch-filtering cancels the harmonic and the heartbeat component.

The measurements that were acquired when the subject was holding breath having the antennas pressed against the body gave the most significant peaks at the true heartbeat rate. Within the frequency band of the heartbeat rate, the frequency component of the vital sign tends to dominate. Such result is presented in Figure 34.

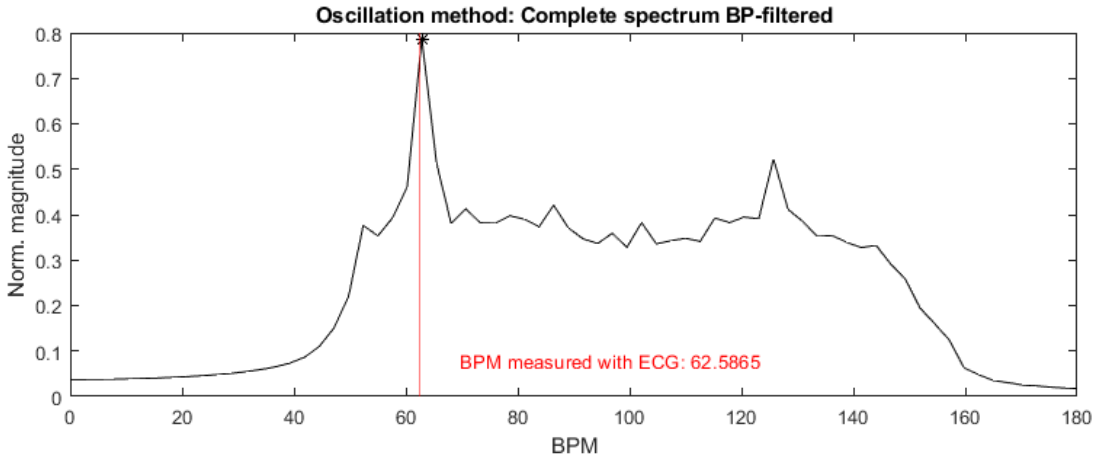

Figure 34. Bandpass filtered signal. Antennas pressed against the chest of the subject. Subject is holding breath.

6. Discussion

The results demonstrated that it is possible to detect vital signs with the investigated system. Hence, the aim of the project was achieved. However, the results were not nearly as good as in previous studies. Previous studies have presented successful results where detection of heartbeat rate was performed at a distance of 1m with a 20cm thick brick wall in between the subject and the measurement system [10]. But then again, the matter of fact is that the system differences regarding both measurement hardware and signal processing makes the comparison unfair. Despite close distance between the antennas and the subject during measurements, only breathing rate was regularly detected. Even at a distance of 50cm, breathing rate could be detected regularly. Unfortunately, longer distances between the measurement system and the subject were not tested in a sufficient amount to claim else. Nevertheless, the maximal trustworthy distance between the subject and the antennas did not exceed 10cm, if the heartbeat rate was to be detected. Moreover, the times at which the heartbeat rate was clearly detected in this study did not occur regularly. The results would somewhat show correct heartbeat rate in an irregular order.

The difference of this study and previous studies is the fact that the measurement systems in the earlier studies have been designed for the purpose of detecting vital signs, whereas the measurement system of this study was designed for medical diagnostics. The major difference between the measurement system of this project and the measurement systems of the previously studied cases is the fact that the latter systems work as impulse radio radars. Impulse radio radars transmit a pulse and the receiver records for a limited time in order to record the echo of the pulse [10] [20]. The investigated system transmits the PN-sequences as UWB-signals repeatedly, demanding somewhat different handling of the signal. Given that the signal types differ, the signal processing methods had to be customized in order to get the desired output. This became a great challenge due to the time limitation.

The general goal of the project was to detect the vital signs after processing the exact same data as the data used for creating images. Small changes in the application of the receiving hardware were necessary in order to make this possible. The rest of the responsibility was put on the signal processing methods. Results have shown that it is possible to monitor the vital signs using provided hardware, which was the main objective of the thesis. However, much can be improved.

An implemented change in the measurement system concerns transferring data from the measurement hardware to the PC. Initially, the program of the setup was designed to transfer data to the PC after each recorded waveform. It took approximately 1 second for each waveform to be recorded and transferred to the PC. The transfer-speed was found to be the bottleneck. The solution to this problem is based on recording and saving an arbitrary number of waveforms on the measurement hardware before finally transferring the data to the PC. This solution makes it impossible to monitor the measurement data in real-time. The problem can be solved by improving the transfer-speed significantly or/and by running some of the signal processing on the measurement hardware to minimize the amount of data to be transferred to the PC.

The most time-demanding part of the project was related to the collection of data. This part includes the modifications of the code for the measurement setup, the design of the robot for controlled displacement and planning and performing all measurements. Limited amount of time prevented further investigation and implementation of algorithms for better processing of the gathered data. Future

improvements should be focused on the signal processing, but also new data could be collected using other antennas with properties similar to the ones used in the true microwave tomography system.

7. Conclusion

The main purpose of the thesis is investigating the possibility to use present system for vital sign detection. The results have proven that it is possible, however only the point-oscillation method could detect the heartbeat rate in the frequency domain.

Considering different positions of the subject at distances up to 50cm, the point oscillation method was able to detect ~90% of the respiration rates compared to ~67% achieved by the cross-correlation method.

The best results for detection of heartbeat rate were acquired when the subject was facing the antenna while holding breath at a distance of 0-10 cm. The point-oscillation method detected the heartbeat rate in 80% of the measurements. Given the same circumstances, the cross-correlation method presented worse results. Only 20% of the outputs would show a frequency corresponding to the true heartbeat rate, which is not reliable. Since, the scenario is that subject is holding breath while sitting still, the main problem is the sensitivity of the measurement system. The measurement system is not always capable of detecting small displacements.

Considering larger displacements such as the displacements generated with the robot setup, or even by breathing, both presented reconstruction methods gave good results regularly. Nevertheless, the results are not often enough good when trying to detect the heartbeat rate to consider studied methods as reliable, therefore there is plenty of space for improvement in the signal processing algorithms.

References

[1] Centers for Disease Control and Prevention, "cdc.gov," Centers for Disease Control and Prevention, 6 September 2017. [Online]. Available: https://www.cdc.gov/vitalsigns/stroke/. [Accessed 19 May 2018].

[2] X. Zeng, A. Fhager, M. Persson and H. Zirath, "Performance Evaluation of a Time-Domain Microwave System for Medical Diagnostics," *Transactions on Intrumentation and Measurement (Early Access),* pp. 1-10, 2018.

[3] Johns Hopkins Medicine, "Johns Hopkins Medicine," [Online]. Available: https://www.hopkinsmedicine.org/healthlibrary/conditions/adult/cardiovascular_diseases/vital_signs_body_temperature_pulse_rate_respiration_rate_blood_pressure_85,P00866. [Accessed 15 May 2018].

[4] Healio, "Healio," [Online]. Available: https://www.healio.com/cardiology/learn-the-heart/ecg-review/ecg-interpretation-tutorial/determining-heart-rate. [Accessed 18 May 2018].

[5] Z. Ge, P. Prasad, N. Costadopoulos, A. Alsadoon, A. K. Singh and A. Elchouemi, "Evaluating the accuracy of wearable heart rate monitors," in *2016 2nd International Conference on Advances in Computing, Communication, & Automation (ICACCA) (Fall)*, Bareilly, India, 2016.

[6] J. Mathew, Y. Semenova and G. Farrel, "A miniature optical breathing sensor," *Biomedical Optics Express,* vol. 3, no. 12, pp. 3325-3331, 2012.

[7] L. Scalise, "Non Contact Heart Monitoring," in *Advances in Electrocardiograms*, INTECH Open Access Publisher, 2012, pp. 82-106.

[8] M. Bartula, T. Tigges and J. Muehlsteff, "Camera-based system for contactless monitoring of respiration," in *2013 35th Annual International Conference of the IEEE Engineering in Medicine and Biology Society (EMBC)*, Osaka, Japan, 2013.

[9] J. Tu, T. Hwang and J. Lin, "Respiration Rate Measurement Under 1-D Body Motion Using Single Continuous-Wave Doppler Radar Vital Sign Detection System," *IEEE Transactions on Microwave Theory and Techniques,* vol. 64, no. 6, pp. 1937-1946, 2016.

[10] A. Lazaro, D. Girbau and R. Villarino, "Analysis of Vital Signs Monitoring using an IR-UWB Radar," *Progress In Electromagnetics Research,* vol. 100, pp. 265-284, 2010.

[11] Lexico, "Definition of microwave in English," Lexico.com, [Online]. Available: https://www.lexico.com/en/definition/microwave. [Accessed 27 October 2019].

[12] Y. Xiao, J. Lin, O. Boric-Lubecke and V. M. Lubecke, "Frequency-Tuning Technique for Remote Detection of Heartbeat and Respiration Using Low-Power Double-Sideband Transmission in the Ka-Band," *IEEE Transactions on Microwave Theory and Techniques,* vol. 54, no. 5, pp. 2023-2032, 2006.

[13] C. Li, Y. Xiao and J. Lin, "Experiment and Spectral Analysis of a Low-Power Ka-Band Heartbeat Detector Measuring From Four Sides of a Human Body," *IEEE Transactions on Microwave Theory and Techniques,* vol. 54, no. 12, pp. 4464-4471, 2006.

[14] X. Zeng, A. Monteith, A. Fhager, M. Persson and H. Zirath, "Investigation of stimulus signals for a time domain microwave imaging system," *IET Microwaves, Antennas & Propagation,* vol. 11, no. 11, pp. 1636-1643, 2017.

[15] A. Monteith, "Improvement of an UWB Time Domain System for Medical Diagnostics," Chalmers University of Technology, Göteborg, Sweden, 2015.

[16] H. Dobsicek Trefna, J. Vrba and M. Persson, "Evaluation of a patch antenna applicator for time reverlsal hyperthemia," *International Journal of Hyperthermia,* vol. 26, no. 2, pp. 185-197, March 2010.

[17] H. Dobsicek Trefna, Y. Yu, A. Fhager, T. McKelvey and M. Persson, "Microwave based decay detection of wood," Chalmers University of Technology, Göteborg.

[18] M. S. Team, "MathWorks.com," MathWorks, 30 August 2018. [Online]. Available: https://se.mathworks.com/matlabcentral/answers/95216-is-lego-mindstorms-nxt-supported-in-previous-releases . [Accessed 9 September 2018].

[19] L. Bengtsson, Elektriska mätsystem och mätmetoder, Lund: Studentlitteratur AB, 2012.

[20] M. Lieb, W. Menzel, B. Schleicher and H. Schumacher, "Vital Signs Monitoring with a UWB Radar Based on a Correlation Receiver," in *Proceedings of the Fourth European Conference on Antennas and Propagation* , Barcelona, Spain, 2010.

[21] X. Zeng, A. Fhager, Z. He, M. Persson, P. Linner and H. Zirath, "Development of a Time Domain Microwave System for Medical Diagnostics," *IEEE Transactions on Instrumentation and Measurement,* vol. 63, no. 12, pp. 2931-2939, 2014.

Appendices

Appendix 1 – Block diagram of the FPGA program

The block diagram below shows the general process of the FPGA. The variable "delay_loops" is a positive integer that takes an arbitrary value chosen by the user.

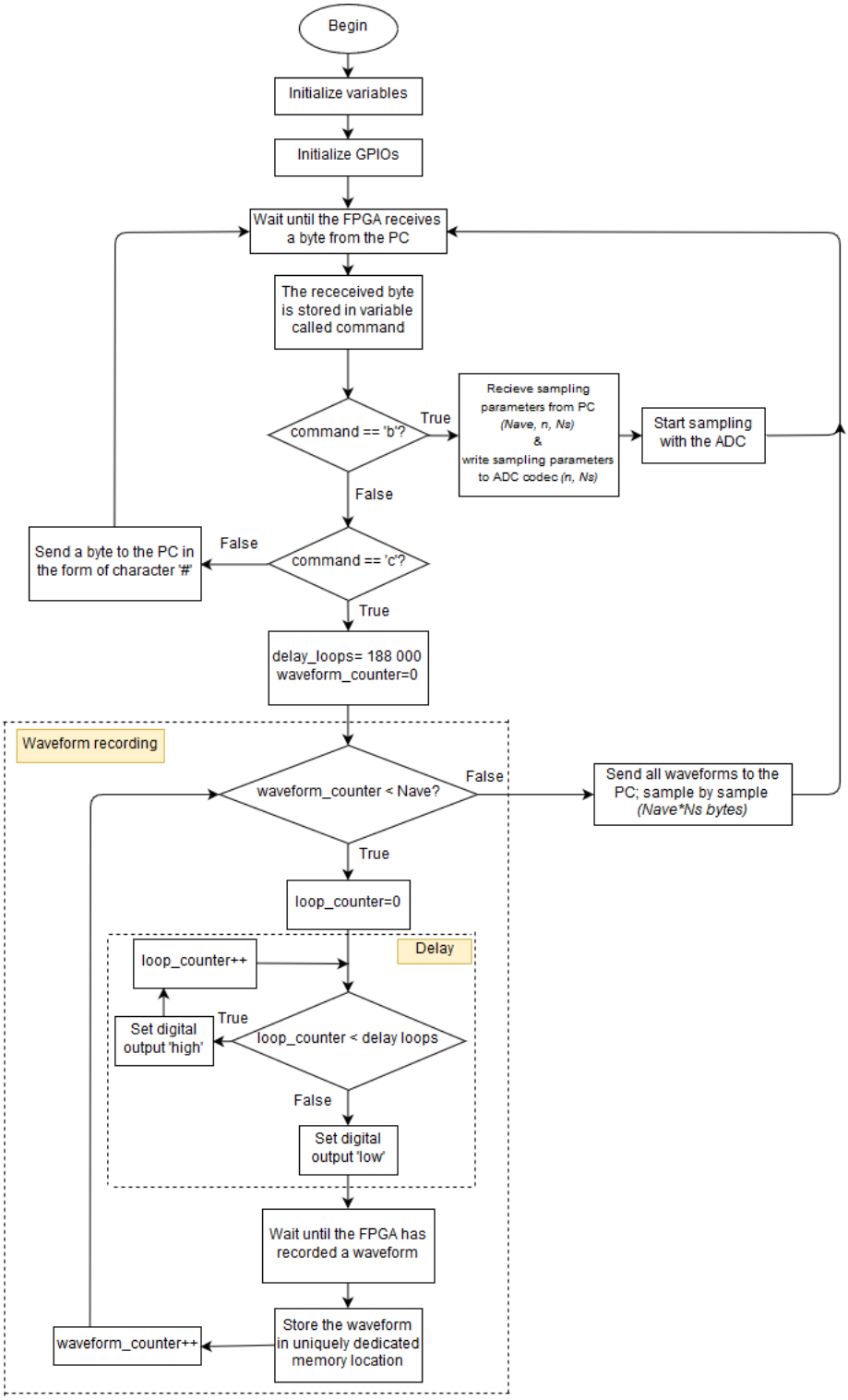

Attachment 1. Block diagram of the FPGA program

Appendix 2 – Simulink model for Lego Mindstorms NXT

The following 2 attachements show the complete program for the Lego Mindstorms NXT controller used in this project.

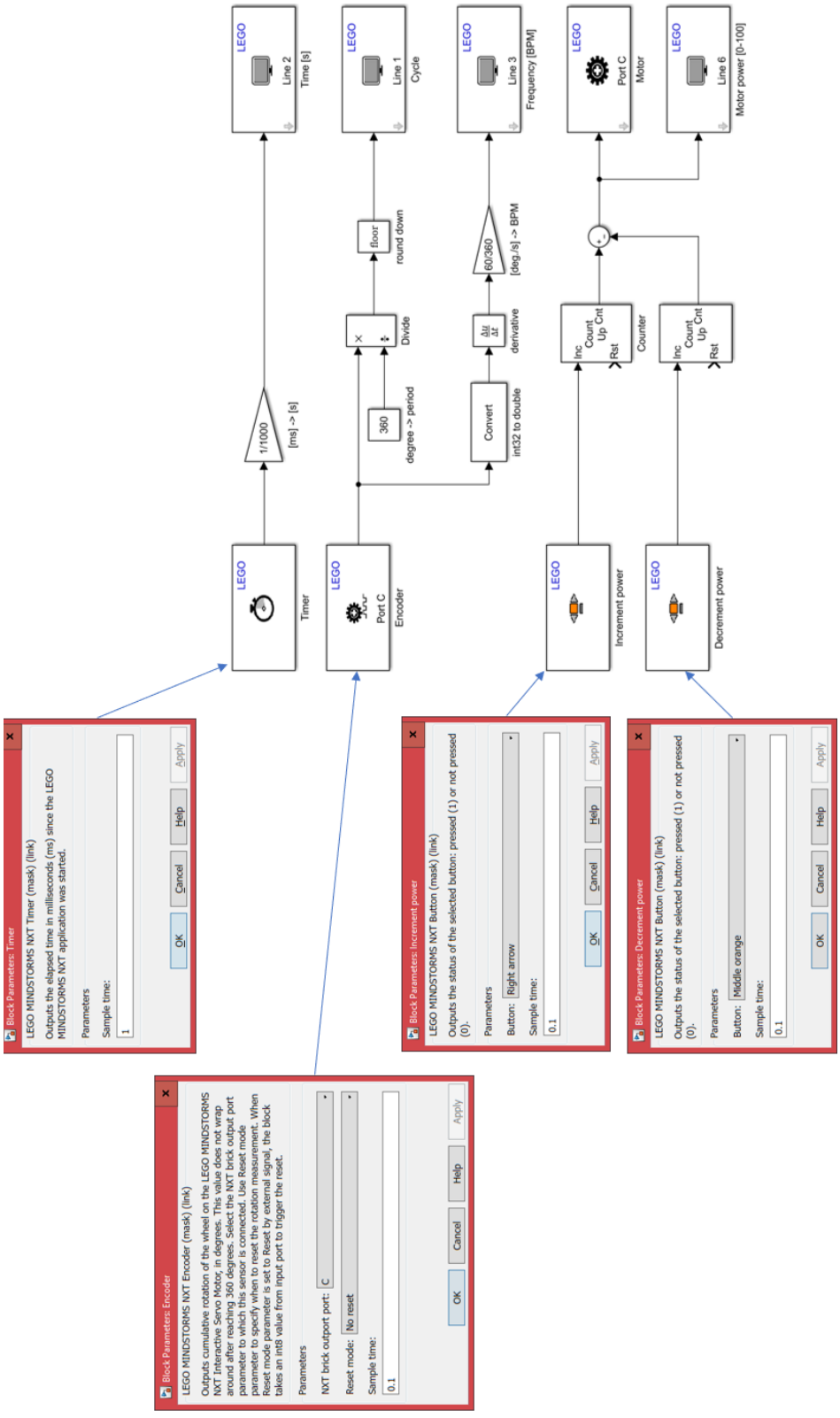

Attachment 2. Lego Mindstorms NXT program. Image 1/2.

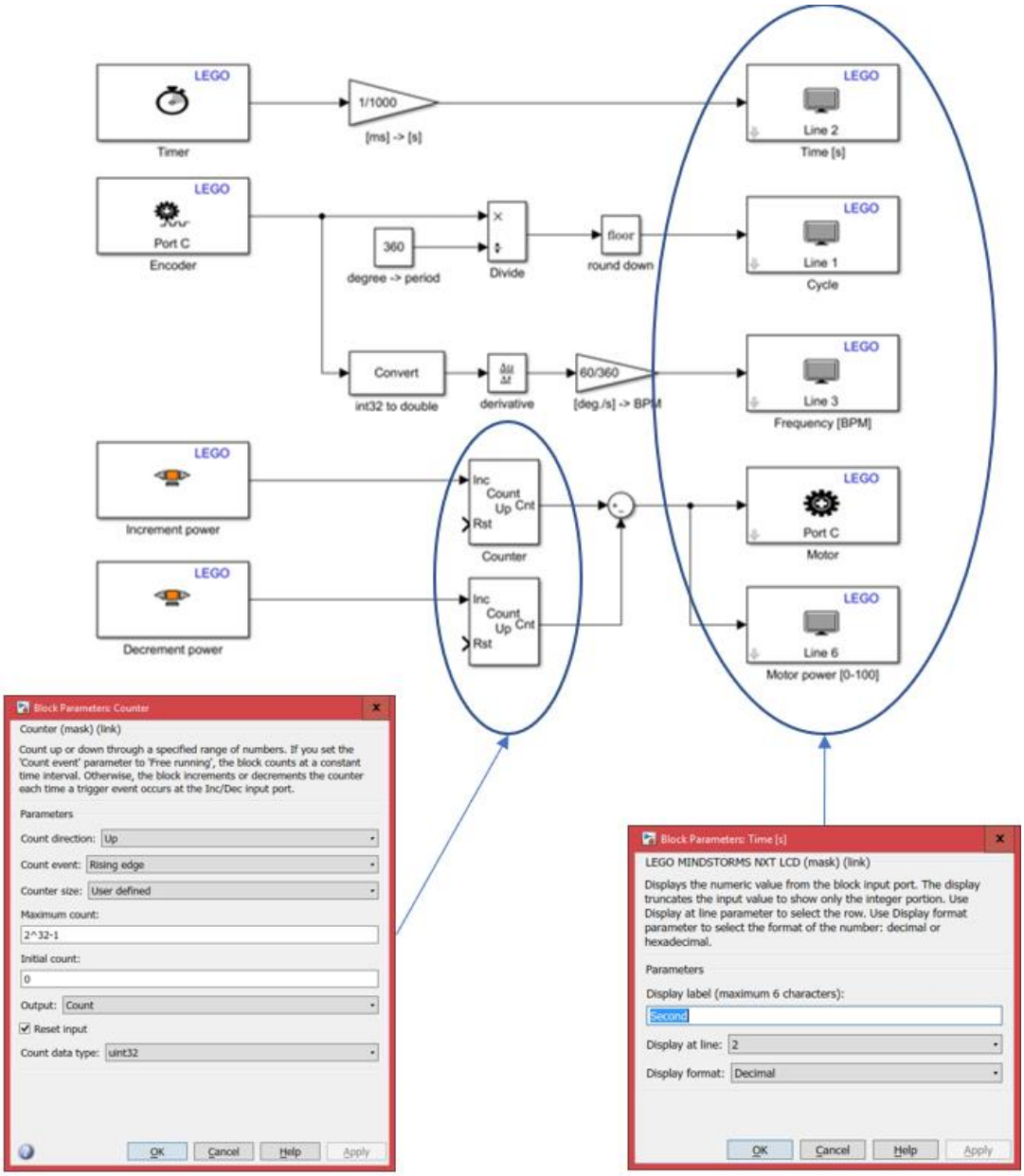

Attachment 3. Lego Mindstorms NXT program. Image 2/2.

Appendix 3 – Operation Manual

To prepare the measurement system, some steps are necessary to carry out. Firstly, the system clock f_b must be set in the PN-sequence generator, before the PN-sequence generator is started. Once the clock is up and running, the settings of the PLL should be set to such that make the PLL output another clock with a frequency, in this case, corresponding to fast-time sampling frequency f_f. The last step is to adjust the phase-shift within the clock distributor to trigger the T/H and the ADC with the right timing [21]. The FPGA handles the sampled data stream coming from the ADC and last of all transfers the data to the PC for processing.